Optimal Power Flow Pursuit via Feedback-Based Safe Gradient Flow

Antonin Colot, *Graduate Student Member, IEEE*, Yiting Chen, Bertrand Cornélusse, Jorge Cortés, *Fellow, IEEE*, and Emiliano Dall'Anese, *Senior Member, IEEE*

***Abstract*— This article considers the problem of controlling inverter-interfaced distributed energy resources (DERs) in a distribution grid to solve an ac optimal power flow (OPF) problem in real time. The ac OPF includes voltage constraints and seeks to minimize costs associated with the economic operation, power losses, or the power curtailment from renewables. We develop an online feedback optimization method to drive the DERs' power setpoints to solutions of an ac OPF problem based only on voltage measurements (and without requiring measurements of the power consumption of noncontrollable assets). The proposed method—grounded on the theory of control barrier functions (CBFs)—is based on a continuous approximation of the projected gradient flow, appropriately modified to accommodate measurements from the power network. We provide results in terms of local exponential stability and assess the robustness to errors in the measurements and in the system Jacobian matrix. We show that the proposed method ensures anytime satisfaction of the voltage constraints when no model and measurement errors are present; if these errors are present and are small, the voltage violation is practically negligible. We also discuss extensions of the framework to virtual power plant (VPP) setups and cases where constraints on power flows and currents must be enforced. Numerical experiments on a 93-bus distribution system with realistic load and production profiles show superior performance in terms of voltage regulation relative to existing methods.**

***Index Terms*— AC optimal power flow (OPF), distributed energy resources (DERs), distribution networks, real-time control.**

I. Introduction

THIS work seeks to contribute to the domain of real-time control and operation of distribution systems with high integration of inverter-interfaced distributed energy resources (DERs). The steady increase in energy costs, combined with government incentives advocating for the utilization of renewable energy sources and energy-efficient automated load control, has reshaped the operation of distribution networks [1], [2]. Historically, distribution networks were designed to manage unidirectional power flows; however, the increased integration of renewable resources and load management strategies led to operational and reliability challenges related to reversed power flows, voltage fluctuations, and power quality.

Traditional techniques based on solving an ac optimal power flow (OPF) problem [3], [4] require collecting information of all noncontrollable powers and running an iterative method; this process may be long compared to the fast-changing conditions of a modern distribution system [1], [2]; existing Volt/Var techniques may not fully resolve voltage regulation and may in fact increase line currents; and recent works on emulating OPF solutions via neural networks can alleviate the computational burden [5], [6] but still require measurements of all the noncontrollable powers (which are the inputs to the neural network) and may not even produce feasible power setpoints.

Collecting measurements of noncontrollable powers in distribution networks in real time (e.g., at the second level) is challenging as distribution systems are historically measurement-scarce, as discussed in [7]. Even though new types of sensing and communication infrastructures can capture real-time data, traditional techniques for solving the ac OPF problem in distribution systems require collecting load measurements in real time from *each* meter and distribution transformer, which is impractical and economically unfeasible [8]. In this work, we focus on real-time ac OPF methods [9], [10], [11], [12], [13], [14] and seek new strategies that exhibit strong performance in terms of achieved operational cost and voltage limit satisfaction (both from analytical and numerical standpoints) while using limited measurements. In particular, we seek methods that do not require a complete ac model and knowledge of all the noncontrollable powers throughout the nodes of the system.

A. Prior Work

Several approaches have been explored to develop real-time OPF algorithms. In general, existing solutions leverage online optimization techniques and incorporate measurements of some network quantities to bypass the need for a system-level model. In the following, we present a list that is by no

Received 12 September 2024; accepted 23 October 2024. This work was supported in part by the National Science Foundation (NSF) under Grant 2444163 and Grant 1947050. The work of Antonin Colot was supported by the Research Fellow Fellowship of the Fonds de la Recherche Scientifique - FNRS. Recommended by Associate Editor F. You. *(Antonin Colot and Yiting Chen contributed equally to this work.) (Corresponding author: Antonin Colot.)*

Antonin Colot is with the Montefiore Institute, University of Liège, 4000 Liège, Belgium, and also with the Department of Electrical, Computer and Energy Engineering, University of Colorado Boulder, Boulder, CO 80309 USA (e-mail: antonin.colot@uliege.be).

Yiting Chen and Emiliano Dall'Anese are with the Department of Electrical and Computer Engineering, Boston University, Boston, MA 02215 USA (e-mail: yich4684@bu.edu; edallane@bu.edu).

Bertrand Cornélusse is with the Montefiore Institute, University of Liège, 4000 Liège, Belgium (e-mail: bertrand.cornelusse@uliege.be).

Jorge Cortés is with the Department of Mechanical and Aerospace Engineering, University of California at San Diego, San Diego, CA 92093 USA (e-mail: cortes@ucsd.edu).

Digital Object Identifier 10.1109/TCST.2024.3504254

means exhaustive. Feedback algorithms using voltage measurements based on linearized models were developed in [9] and recently [15] combined with data-driven learning to synthesize decentralized strategies; online primal-dual methods with voltage and/or power measurements have been proposed in [10] and [16]; and model-free counterparts were proposed in [17] and [18]. Discrete-time projected gradient algorithms for the OPF problem are employed in [13] and [19], while projected gradient flows were used in [11]. Projection of gradient iterates onto a linearization of the feasible set around the current state was used in [14] for reactive power control. Power control for aggregations of DERs to track setpoints at the point of common coupling via gradient-type methods was proposed in, e.g., [20]. Online quasi-Newton methods were used in [21], and online interior-point methods were proposed in [22]. In addition to [9], distributed methods were explored in, e.g., [23].

B. Contributions

Compared to the works in the context of real-time OPF methods mentioned above, the contributions of our article can be described as follows.

(c1) We propose a new approach for the design of real-time OPF algorithms, which is grounded on the theory of control barrier functions (CBFs) [24]. We leverage a continuous approximation of projected gradient flows [25], appropriately modified to accommodate voltage measurements from the power network. Inheriting the properties of CBF methods, the proposed algorithm—here termed feedback-based safe gradient flow (SGF)—ensures anytime satisfaction of the voltage constraints while reaching solutions of the OPF.

(c2) From a theoretical standpoint, we show that the proposed feedback-based SGF renders isolated optimal solutions of the ac OPF problem locally exponentially stable and ensures the anytime satisfaction of the voltage constraints. On the other hand, existing feedback-based optimization methods for distribution systems [9], [10], [11], [12], [13], [14] do not guarantee anytime satisfaction of the voltage constraints.

(c3) We provide results in terms of practical exponential stability and practical forward invariance when voltage measurements are affected by errors and when the Jacobian matrix of the ac power flow equations is computed only approximately (for example, when a linear approximation of the power flow equations is used).

(c4) We perform numerical experiments on a 93-bus distribution system [26] and with realistic load and solar production profiles from the Open Power System Data. We show that our method shows far superior performance in terms of voltage regulation relative to existing online primal-dual methods and Volt/Var strategies.

We note that relative to [14], our design leverages the theory of CBFs [24], [25], our method can handle constraints that are nonlinear, and we provide practical stability and forward-invariance guarantees.

From a practical standpoint, we provide remarks throughout this article on how the proposed method can be integrated into the existing distribution system infrastructure, for instance, by leveraging DER management systems (DERMSs) for distribution operators and existing communication infrastructure or a supervisory control and data acquisition (SCADA) system.

II. Problem Formulation

Notations: Uppercase (lowercase) boldface letters are used for matrices (column vectors), $(.)^\top$ denotes the transposition, and $(.)^*$ the complex conjugate; j denotes the imaginary unit, and $|.|$ denotes the absolute value of a number. If we consider a given vector $\boldsymbol{x} \in \mathbb{R}^N$, $\text{diag}(\cdot)$ returns a $N \times N$ matrix with the element of $\boldsymbol{x}$ in its diagonal. For vectors $\boldsymbol{x} \in \mathbb{R}^n$ and $\boldsymbol{u} \in \mathbb{R}^m$, $\|\boldsymbol{x}\|$ denotes the ℓ_2-norm, and $(\boldsymbol{x}, \boldsymbol{u}) \in \mathbb{R}^{n+m}$ denotes their vector concatenation. We denote as $\mathbb{0}$ a vector or matrix with all zeros (the dimensions will be clear from the context). $\mathbb{C}$ denotes the set of complex numbers, and for a vector $\boldsymbol{x} \in \mathbb{C}^N$, $\Re(\boldsymbol{x}) \in \mathbb{R}^N$ denotes its real part and $\Im(\boldsymbol{x}) \in \mathbb{R}^N$ denotes its imaginary part.

A. Distribution System Model

Consider an electrical distribution system with $N+1$ nodes and hosting G DERs; these may include inverter-interfaced photovoltaic (PV) systems, energy storage systems, variable-speed drives, and electric vehicles or small-scale generators if any. The node 0 is taken to be the substation or the point of common coupling, while $\mathcal{N} := \{1, \ldots, N\}$ is the set of remaining nodes. We consider a steady-state model where voltages and currents are represented in the phasor domain. Accordingly, let $v_k = v_k e^{j\delta_k} \in \mathbb{C}$, $v_k := |v_k|$, and $i_k = |i_k| e^{j\psi_k} \in \mathbb{C}$ be the line-to-ground voltage and current injected at node i, respectively. Moreover, the voltage at node 0 is set to $v_0 = V_0 e^{j\delta_0}$ [27].

Using Ohm's law and Kirchhoff's law, one has the usual phasor relationship

$$\begin{bmatrix} i_0 \\ \boldsymbol{i} \end{bmatrix} = \begin{bmatrix} y_0 & \bar{\boldsymbol{y}}^T \\ \bar{\boldsymbol{y}} & \boldsymbol{Y} \end{bmatrix} \begin{bmatrix} v_0 \\ \boldsymbol{v} \end{bmatrix} \tag{1}$$

where $\boldsymbol{v} \in \mathbb{C}^N$ collects the voltages $\{v_k\}_{k\in\mathcal{N}}$, $\boldsymbol{i} \in \mathbb{C}^N$ collects the currents $\{i_k\}_{k\in\mathcal{N}}$, and $\boldsymbol{Y} \in \mathbb{C}^{N\times N}$, $\bar{\boldsymbol{y}} \in \mathbb{C}^N$, and $y_0 \in \mathbb{C}$ are based on the series and shunt admittances of the distribution lines represented by a standard Π-model (see, for example, [27], [28]). Using (1), it is possible to relate complex powers at the nodes $\mathcal{N}$ with voltages as

$$\boldsymbol{s} = \text{diag}(\boldsymbol{v}) \left(\bar{\boldsymbol{y}}^* v_0^* + \boldsymbol{Y}^* \boldsymbol{v}^* \right) \tag{2}$$

where $\boldsymbol{s} = \boldsymbol{p}_{\text{net}} + j\boldsymbol{q}_{\text{net}} \in \mathbb{C}^N$, with $\boldsymbol{p}_{\text{net}} = [p_{\text{net},1}, \ldots, p_{\text{net},N}]^\top$ and $\boldsymbol{q}_{\text{net}} = [q_{\text{net},1}, \ldots, q_{\text{net},N}]^\top$ vectors collecting the net active and reactive power injections at nodes $\mathcal{N}$. Note that $\boldsymbol{p}_{\text{net}}$ and $\boldsymbol{q}_{\text{net}}$ account for both the powers (injected or consumed) of the DERs and the aggregate powers of the noncontrollable loads that are connected to each of the nodes $\mathcal{N}$. In particular, let $\boldsymbol{p}_l := [p_{l,1}, \ldots, p_{l,N}]^\top \in \mathcal{W}_p$, $\boldsymbol{q}_l := [q_{l,1}, \ldots, q_{l,N}]^\top \in \mathcal{W}_q$ with compact sets $\mathcal{W}_p \subset \mathbb{R}^N$ and $\mathcal{W}_q \subset \mathbb{R}^N$ be vectors collecting the net active and reactive power consumed at the nodes by noncontrollable devices (positive when the power is consumed). For the G DERs, consider the vector $\boldsymbol{u} = [p_1, p_2, \ldots, p_G, q_1, q_2, \ldots, q_G]^\top$ collecting their active and

reactive powers (with a positive sign denoting generation). Moreover, let $\mathcal{G} := \{1, \dots, G\}$ be the index for the DERs, and define a function $m : \mathcal{G} \to \mathcal{N}$, which maps a DER index to the node where the DER is connected to. With this notation, note that $\mathcal{G}_n := \{i \in \mathcal{G} : n = m(i)\}$ is the set of DERs connected at node $n \in \mathcal{N}$. Then, the net active and reactive powers are given by $p_{\text{net},n} = \sum_{j\in\mathcal{G}_n} p_j - p_{l,n}$ and $q_{\text{net},n} = \sum_{j\in\mathcal{G}_n} q_j - q_{l,n}$ at each n. In what follows, we consider a set of nodes $\mathcal{M} \subseteq \mathcal{N}$ with cardinality $M = |\mathcal{M}|$ where voltages are to be regulated (if the operator would like to monitor and regulate all the voltages, then $\mathcal{M} = \mathcal{N}$). Finally, let $\mathcal{U}_i \subset \mathbb{R}^2$ be a compact set of admissible power setpoints such that $(p_i, q_i) \in \mathcal{U}_i$ for $i \in \mathcal{G}$. We define $\mathcal{U} := \mathcal{U}_1 \times \mathcal{U}_2 \times \cdots \times \mathcal{U}_G$ so that $\boldsymbol{u} \in \mathcal{U}$.

Equation (2) describes the power flow equations. For a given vector of net power injection $\boldsymbol{s}$, one can solve this nonlinear system of equations using numerical methods to find the vector of voltage phasors $\boldsymbol{v}$. Notice that the system of equations (2) may have no, one, or many solutions. For the rest of this article, we make the following assumption when restricting to a neighborhood of the nominal voltage profile.

Assumption 1 (Mapping in a Neighborhood of the Nominal Voltage Profile): There exists a unique continuously differentiable function $H : \mathcal{U} \times \mathcal{W}_p \times \mathcal{W}_q \to \mathbb{R}^M$ such that $H_i(\boldsymbol{u}; \boldsymbol{p}_l, \boldsymbol{q}_l) = v_i = |v_i|$ for $i \in \mathcal{M}$. The Jacobian $J_H(\boldsymbol{u}; \boldsymbol{p}_l, \boldsymbol{q}_l) := (\partial H(\boldsymbol{u}; \boldsymbol{p}_l, \boldsymbol{q}_l)/\partial \boldsymbol{u})$ is locally Lipschitz continuous. □

If multiple solutions exist, we only consider the *practical* solution, i.e., in the neighborhood of the nominal voltage profile, we restrict the attention to the solution that leads to high voltages and small line currents. The existence of the map H is based on the implicit function theorem and the results of, e.g., [28], [29], [30] for single-phase and multiphase distribution networks.

Remark 1 (Jacobian of Map H): For the sake of generality, we write the Jacobian $J_H(\boldsymbol{u}; \boldsymbol{p}_l, \boldsymbol{q}_l)$ as dependent on the controllable and noncontrollable power injections. However, in this article, we will leverage approximations of the Jacobian matrix; these estimates can be obtained without any knowledge of noncontrollable power injections. We will provide remarks on linear approximations in Section III-B. □

Remark 2 (Model and Notation): It is important to note that the framework proposed in this article works for multiphase distribution systems with both wye and delta connections under the same Assumption 1. The existence of the map H for unbalanced multiphase networks is discussed in [30]. However, to simplify the notation and streamline the exposition, we outline the framework using a single-phase model. □

B. OPF for Voltage Regulation in Distribution Systems

In this section, we outline a formulation of the OPF problem for distribution systems. By solving an OPF problem, one seeks power setpoints for the DERs that minimize the operational cost (or maximize performance objectives) for the utilities and the customers, subject to operational constraints that may include voltage limits, line ampacity, or hardware limits [3], [4]. The cost associated with the utility companies may favor the minimization of system losses or the usage of controllable resources or may perform voltage regulation (e.g., thus including the cost of active power curtailment or reactive power compensation [9], [23]); on the other hand, customers may want to minimize the power curtailed by renewables or maximize their revenue by providing ancillary services.

To outline our framework, we start with the following formulation of the OPF problem (we present some extensions later in Section III-D):

$$\begin{aligned} \min_{\boldsymbol{v}\in\mathbb{R}^M, \boldsymbol{u}\in\mathbb{R}^{2G}} \quad & C_v(\boldsymbol{v}) + C_p(\boldsymbol{u}) \\ \text{s.t. } & \underline{V} \le v_i \le \bar{V} \qquad \forall i \in \mathcal{M} \\ & v_i = H_i(\boldsymbol{u}; \boldsymbol{p}_l, \boldsymbol{q}_l) \quad \forall i \in \mathcal{M} \\ & (p_i, q_i) \in \mathcal{U}_i \quad \forall i \in \mathcal{G} \end{aligned} \tag{3}$$

where the functions $C_v : \mathbb{R}^M \to \mathbb{R}$ and $C_p : \mathbb{R}^{2G} \to \mathbb{R}$ have locally Lipschitz continuous gradients, $\underline{V}$ and $\bar{V}$ are predefined voltage bounds that the operator wants to enforce at nodes $i \in \mathcal{M}$, and $H_i(\boldsymbol{u}; \boldsymbol{p}_l, \boldsymbol{q}_l)$ is the ith component of the function $H(\boldsymbol{u}; \boldsymbol{p}_l, \boldsymbol{q}_l)$ (specifying the voltage magnitude v_i). We note that (3) can be equivalently rewritten as

$$\begin{aligned} \min_{\boldsymbol{u}\in\mathbb{R}^{2G}} \quad & C_v(H(\boldsymbol{u}; \boldsymbol{p}_l, \boldsymbol{q}_l)) + C_p(\boldsymbol{u}) \\ \text{s.t. } & \underline{V} \le H_i(\boldsymbol{u}; \boldsymbol{p}_l, \boldsymbol{q}_l) \le \bar{V} \quad \forall i \in \mathcal{M} \\ & (p_i, q_i) \in \mathcal{U}_i \quad \forall i \in \mathcal{G} \end{aligned} \tag{4}$$

where $\boldsymbol{u}$ is the only optimization variable. Hereafter, we assume that the set $\mathcal{U}_i$ can be expressed as

$$\mathcal{U}_i = \{(p_i, q_i) \in \mathbb{R}^2 : \ell_i(p_i, q_i) \le \mathbb{0}_{n_{c_i}}\} \tag{5}$$

where $\ell_i : \mathbb{R}^2 \to \mathbb{R}^{n_{c_i}}$ is a vector-valued function modeling power limits and the inequality is taken entrywise. For example, if the ith DER is an inverter-interfaced controllable renewable source, then $\ell_i(p_i, q_i) = [p_i^2 + q_i^2 - s_{n,i}^2, p_i - p_{\max,i}, -p_i]^\top$, where $s_{n,i}$ and $p_{\max,i}$ denote the inverter rated size and the maximum available active power, respectively; that is, $\mathcal{U}_i = \{(p_i, q_i) \in \mathbb{R} : p_i^2 + q_i^2 \le s_{n,i}^2, p_i \le p_{\max,i}, p_i \ge 0\}$. Moreover, we denote as

$$\mathcal{F} := \{\boldsymbol{u} : \underline{V} \le H_i(\boldsymbol{u}; \boldsymbol{p}_l, \boldsymbol{q}_l) \le \bar{V}, \forall i \in \mathcal{M}, \boldsymbol{u} \in \mathcal{U}\} \tag{6}$$

the feasible set of (4). We impose the following assumption on (4), which is typical in the ac OPF context.

Assumption 2 (Regularity of Isolated Solutions): Assume that (4) is feasible, and let $\boldsymbol{u}^*$ be a local minimizer and an isolated Karush–Kuhn–Tucker (KKT) point for (4) for given $\boldsymbol{p}_l, \boldsymbol{q}_l$. Assume that the following holds.

1) Strict complementarity slackness [31] and the linear independence constraint qualification (LICQ) [32] hold at $\boldsymbol{u}^*$.
2) The maps $\boldsymbol{u} \mapsto C_p(\boldsymbol{u})$, $\boldsymbol{u} \mapsto C_v(H(\boldsymbol{u}; \boldsymbol{p}_l, \boldsymbol{q}_l))$ and $\boldsymbol{u} \mapsto H(\boldsymbol{u}; \boldsymbol{p}_l, \boldsymbol{q}_l)$ are twice continuously differentiable over some open neighborhood $\mathcal{B}(\boldsymbol{u}^*, r_1) := \{\boldsymbol{u} : \|\boldsymbol{u} - \boldsymbol{u}^*\| < r_1\}$ of $\boldsymbol{u}^*$, and their Hessian matrices are positive semidefinite at $\boldsymbol{u}^*$.
3) The Hessian $\nabla^2 C_p(\boldsymbol{u}^*)$ is positive definite. □

Assumption 2 imposes some mild regularity assumptions on a neighborhood of a strict locally optimal solution. If (4) is formulated based on the linearized ac power flow equations [9],

[10] and the cost is strongly convex, then Assumption 2 is satisfied. For the most general nonlinear ac OPF problem [21], Assumption 2 is supported by the results of [32], where LICQ is investigated.

Problem (4) can be solved using traditional optimization methods for nonlinear programs. However, *(c1)* these batch methods require collecting measurements of all the *noncontrollable* powers $\boldsymbol{p}_l, \boldsymbol{q}_l$ in a distribution network that is known to be historically measurement-scarce [7]; moreover, *(c2)* the time required to collect the measurements of the noncontrollable powers (if available in real time) and run an iterative method to convergence may be long compared to the fast-changing conditions of a modern distribution system [1], [2]. Although recent work on neural networks for ac OPF can alleviate the computational burden (see, e.g., the representative works [5], [6]), they still require measurements of all the noncontrollable powers $\boldsymbol{p}_l, \boldsymbol{q}_l$ as in *(c1)*, and they often rely on heuristics to return a feasible solution. Motivated by the challenges *(c1)–(c2)* and by the need to generate power setpoints that ensure the satisfaction of voltage limits even under uncertain and time-varying operational setups, in this article, we seek to solve to the following problem.

Problem 1: Design an online feedback-optimization algorithm that drives the DERs' power setpoints $\boldsymbol{u}$ to solutions of the problem (4) while ensuring that voltage constraints are always met. The feedback optimization method should use measurements of the voltages instead of requiring knowledge of the noncontrollable powers $\boldsymbol{p}_l, \boldsymbol{q}_l$. □

We note that in Problem 1, we focus on voltage measurements because (4) includes voltage constraints; if (4) is modified to include cost and constraints associated with power flows or currents, then the feedback optimization method would require measurements of those quantities too [16].

From a practical standpoint, in this article, we focus on feedback-optimization algorithms that are implemented in a centralized unit; for instance, these algorithms can be integrated into a DERMS for distribution operators. We also assume that the unit implementing our feedback-based online algorithm has access to synchronized voltage measurements at nodes where voltage constraints are enforced and can transmit new power setpoints to the DERs. This can be done by leveraging existing communication and metering infrastructure or through a SCADA system.

III. Safe OPF Pursuit

A. Feedback-Based Online Algorithm

To solve our regulation problem, we propose the following feedback-based algorithm:

$$\dot{\boldsymbol{u}} = \eta F_\beta(\boldsymbol{u}, \tilde{\boldsymbol{v}}) \tag{7}$$

$$\begin{aligned} F_\beta(\boldsymbol{u}, \tilde{\boldsymbol{v}}) := \arg\min_{\boldsymbol{\theta}\in\mathbb{R}^{2G}} \ & \|\boldsymbol{\theta} + \nabla C_p(\boldsymbol{u}) + J_H(\boldsymbol{u}; \boldsymbol{p}_l, \boldsymbol{q}_l)^\top \nabla C_v(\tilde{\boldsymbol{v}})\|^2 \\ \text{s.t.} \ & -\nabla H_i(\boldsymbol{u}; \boldsymbol{p}_l, \boldsymbol{q}_l)^\top \boldsymbol{\theta} \le -\beta\big(\underline{V} - \tilde{v}_i\big) \quad \forall i \in \mathcal{M} \\ & \nabla H_i(\boldsymbol{u}; \boldsymbol{p}_l, \boldsymbol{q}_l)^\top \boldsymbol{\theta} \le -\beta\big(\tilde{v}_i - \bar{V}\big) \quad \forall i \in \mathcal{M} \\ & J_{\ell_i}(p_i, q_i)^\top \boldsymbol{\theta} \le -\beta \ell_i(p_i, q_i) \quad \forall i \in \mathcal{G} \end{aligned} \tag{8}$$

where $\tilde{v}_i$ is a measurement of $|v_i|$ at node i, $J_H(\boldsymbol{u}; \boldsymbol{p}_l, \boldsymbol{q}_l)$ is the Jacobian matrix of $H(\boldsymbol{u}; \boldsymbol{p}_l, \boldsymbol{q}_l)$, $\nabla H_i(\boldsymbol{u}; \boldsymbol{p}_l, \boldsymbol{q}_l) = [\{(J_H(\boldsymbol{u}; \boldsymbol{p}_l, \boldsymbol{q}_l))_{i,j}\}_{j\in\mathcal{G}}]^\top$ is a $2G \times 1$ vector collecting the entries of $J_H(\boldsymbol{u}; \boldsymbol{p}_l, \boldsymbol{q}_l)$ in the ith row and columns corresponding to nodes in $\mathcal{G}$, $J_{\ell_i}(p_i, q_i)$ is the Jacobian of $(p_i, q_i) \mapsto \ell_i(p_i, q_i)$, $\beta > 0$ is a design parameter, and $\eta > 0$ is the controller gain and is a design parameter. For given $\boldsymbol{u}$ and $\tilde{\boldsymbol{v}}$, problem (8) is a convex quadratic program (QP) with a strongly convex cost; it can be efficiently solved using standard or high-performance embedded solvers for QPs, e.g., [33].

The online feedback optimization algorithm (7) is inspired by CBFs methods [24] and the SGF in [25]; we provide more details on the CBF-based design in Appendix A. In particular, (7) is an approximation of the projected gradient flow $\dot{\boldsymbol{u}} = \text{proj}_{T_{\mathcal{F}}(\boldsymbol{u})}\{-\nabla C_p(\boldsymbol{u}) - J_H^\top \nabla C_v(H(\boldsymbol{u}; \boldsymbol{p}_l, \boldsymbol{q}_l))\}$, where $T_{\mathcal{F}}(\boldsymbol{u})$ is the tangent cone of $\mathcal{F}(\boldsymbol{u})$ at $\boldsymbol{u}$; in fact, one can show [25, Proposition 4.4] that $\lim_{\beta\to\infty} F_\beta(\boldsymbol{u}, H(\boldsymbol{u}; \boldsymbol{p}_l, \boldsymbol{q}_l)) = \text{proj}_{T_{\mathcal{F}}(\boldsymbol{u})}\{-\nabla C_p(\boldsymbol{u}) - J_H^\top \nabla C_v(H(\boldsymbol{u}; \boldsymbol{p}_l, \boldsymbol{q}_l))\}$.

The algorithm (7) is designed to steer the power setpoints of the DERs $\boldsymbol{u}$ to optimal solutions of the ac OPF while continuously guaranteeing feasibility (i.e., satisfaction of voltage limits). As shown in Fig. 1, (7) effectively acts as a feedback controller by replacing the voltage *model* $H(\boldsymbol{u}; \boldsymbol{p}_l, \boldsymbol{q}_l)$ with *measurements* $\tilde{\boldsymbol{v}}$ of the voltage magnitudes that automatically satisfy the power flow equations [21], [34]. This is a key modification that allows one to avoid collecting measurements of $\boldsymbol{p}_l, \boldsymbol{q}_l$ [9], [10], [16]. However, we note that (7) requires the computation of the Jacobian matrix of $H(\boldsymbol{u}; \boldsymbol{p}_l, \boldsymbol{q}_l)$. One cannot derive an explicit formulation of the Jacobian matrix of $H(\boldsymbol{u}; \boldsymbol{p}_l, \boldsymbol{q}_l)$ as this map does not have an analytical formulation. Therefore, we modify (7) as follows:

$$\dot{\boldsymbol{u}} = \eta \hat{F}_\beta(\boldsymbol{u}, \tilde{\boldsymbol{v}}) \tag{9}$$

$$\begin{aligned} \hat{F}_\beta(\boldsymbol{u}, \tilde{\boldsymbol{v}}) := \arg\min_{\boldsymbol{\theta}\in\mathbb{R}^{2G}} \ & \big\|\boldsymbol{\theta} + \nabla C_p(\boldsymbol{u}) + J_{\hat{H}}^\top \nabla C_v(\tilde{\boldsymbol{v}})\big\|^2 \\ \text{s.t.} \ & -\nabla \hat{H}_i^\top \boldsymbol{\theta} \le -\beta\big(\underline{V} - \tilde{v}_i\big) \quad \forall i \in \mathcal{M} \\ & \nabla \hat{H}_i^\top \boldsymbol{\theta} \le -\beta\big(\tilde{v}_i - \bar{V}\big) \quad \forall i \in \mathcal{M} \\ & J_{\ell_i}(\boldsymbol{u})^\top \theta \le -\beta \ell_i(p_i, q_i) \quad \forall i \in \mathcal{G} \end{aligned} \tag{10}$$

where $J_{\hat{H}}$ and $\{\hat{H}_i\}_{i\in\mathcal{M}}$ are estimates or approximations of J_H and $\{H_i\}_{i\in\mathcal{M}}$, respectively. These estimates can be obtained using online estimation methods (see, e.g., [35], [36]), or they can be computed based on a linear approximation of the ac power flow equations of the form

$$\hat{H}_n(\boldsymbol{u}; \boldsymbol{p}_l, \boldsymbol{q}_l) = \sum_{i\in\mathcal{G}} (r_{n,m(i)} p_i + b_{n,m(i)} q_i) + c_n(\boldsymbol{p}_l, \boldsymbol{q}_l) \tag{11}$$

$n \in \mathcal{N}$, where the coefficients $\{r_{n,m(i)}, b_{n,m(i)}\}_{i\in\mathcal{G}}$ can be found, as explained in e.g., [9], [28], [29], [37], [38] (note that linear approximations of the power flow equations are available for both single-phase and unbalanced multiphase distribution networks). We will provide more remarks on the linear approximation shortly in Section III-B.

The proposed feedback-based SGF is summarized in Algorithm 1 and illustrated in Fig. 1.

In terms of implementation of Algorithm 1, we highlight the following practical aspects.

1) The main step [S2a] is performed at a central unit (i.e., the blue box in Fig. 1). This central unit can be

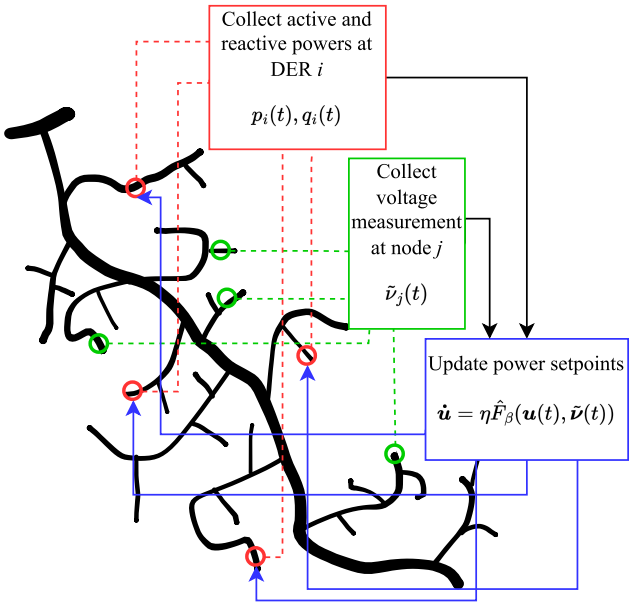

Fig. 1. Closed-loop implementation of the proposed online feedback optimization algorithm. A central unit (blue box) receives measurements of voltages (from measurement units, green box) and the DERs' output powers from inverters (red box); based on these measurements, it updates the DERs' setpoints based on the proposed controller $\dot{\boldsymbol{u}}(t) = \eta \hat{F}_\beta(\boldsymbol{u}(t), \tilde{\boldsymbol{v}}(t))$. Once the setpoints $\boldsymbol{u}(t)$ are computed, the central unit transmits $\boldsymbol{u}(t)$ to the DERs' inverters. Through this closed-loop scheme, the proposed controllers drive the distribution system to solutions of the ac OPF problem (4).

Algorithm 1 Feedback-Based SGF

Initialization: Compute $J_{\hat{H}}$ and $\{\hat{H}_i, i \in \mathcal{M}\}$. Set $\beta > 0$, $\eta > 0$.

Real-time operation: for $t \geq 0$, repeat:

[S1a] Measure output powers $\{p_i(t), q_i(t), i \in \mathcal{G}\}$

[S1b] Measure voltages $\{\tilde{v}_i(t), i \in \mathcal{M}\}$

[S2a] Update power setpoints via $\dot{\boldsymbol{u}}(t) = \eta \hat{F}_\beta(\boldsymbol{u}(t), \tilde{\boldsymbol{v}}(t))$

[S2b] Implement setpoints $\boldsymbol{u}(t)$

Go to [S1a] and [S1b]

integrated, for example, into a DERMS or an advanced distribution management system for distribution operators. After performing step [S2a], the central unit sends the updated setpoints to the DERs' inverters.

2) Step [S1a] is performed at the DERs (a DER is represented by a red box in Fig. 1); the inverters measure the output powers $\{p_i(t), q_i(t), i \in \mathcal{G}\}$ and send the measurements to the central unit. The inverters also implement step [S2b] after they receive the setpoints from the central unit.
3) The SGF (9) relies on measurements of the voltages at the network locations $\mathcal{M}$, as required in the step [S1b]. It is assumed that those measurements are obtained in real time using sensing devices communicating with the centralized controller, e.g., μPMUs [39], or through the advanced metering infrastructure (a meter is represented by a green box in Fig. 1).

In practice, the proposed measurement-based SGF (9) can be implemented with discretization (similar to well-established CBF-based methods [24]). The discretization interval depends on the time required to collect voltage measurements and solve the QP. Linearly constrained convex QP programs are known to be solved efficiently (e.g., in milliseconds) by both existing open-source solvers (such as IPOPT) and commercial solvers. Synchronized voltage measurements can be obtained via SCADA at a fast scale (i.e., second or subsecond level) [7], [39].

Remark 3 (Pseudo-Measurements): Our framework is applicable to the case where the system operator may utilize a mix of actual voltage measurements and pseudo-measurements [40]. For example, suppose that the system operator can measure voltages at some nodes $\mathcal{M}_{\text{meter}} \subset \mathcal{M}$ and relies on pseudo-measurements at the other nodes. Then,

$$\tilde{v}_i = \begin{cases} H_i(\boldsymbol{u}; \boldsymbol{p}_l, \boldsymbol{q}_l) + n_i, & i \in \mathcal{M}_{\text{meter}} \\ H_{i,\text{pseudo}}(\boldsymbol{u}; \boldsymbol{p}_l, \boldsymbol{q}_l), & i \in \mathcal{M} \setminus \mathcal{M}_{\text{meter}} \end{cases} \tag{12}$$

where n is a bounded measurement noise and $H_{i,\text{pseudo}}(\boldsymbol{u}; \boldsymbol{p}_l, \boldsymbol{q}_l)$ represents a model used to generate the pseudo-measurements (i.e., using a state estimator). □

Remark 4 (Measurement of Setpoints): If the embedded controllers of inverters are guaranteed to implement the power setpoints, in principle, the step [S1a] in Algorithm 1 is not needed. However, the operator may want to measure current setpoints $\{p_i(t), q_i(t), i \in \mathcal{G}\}$ for verification purposes and to monitor the state of the DERs' inverters. □

B. Remarks on the Linear Model

In the following, we comment on the linear approximation used in this article. We start with the power flow equations (2) that we linearize around a given voltage profile $\bar{\boldsymbol{v}} = [\bar{v}_1, \ldots, \bar{v}_N]^\top$. Let us consider $\boldsymbol{d} \in \mathbb{R}^N$ capturing the deviations around the linearization point. We have

$$\begin{aligned} \boldsymbol{s} = \text{diag}(\bar{\boldsymbol{v}} + \boldsymbol{d})\left(\bar{\boldsymbol{y}}^* v_0^* + \boldsymbol{Y}^* \bar{\boldsymbol{v}}^*\right) + \text{diag}(\boldsymbol{d})\left(\boldsymbol{Y}^* \bar{\boldsymbol{v}}^*\right) \\ + \text{diag}(\boldsymbol{d})\left(\boldsymbol{Y}^* \boldsymbol{d}^*\right). \end{aligned} \tag{13}$$

If we discard the second-order terms $\text{diag}(\boldsymbol{d})(\boldsymbol{Y}^* \boldsymbol{d}^*)$ and consider the following choice for the nominal voltage profile:

$$\bar{\boldsymbol{v}} = -\boldsymbol{Y}^{-1} \bar{\boldsymbol{y}} v_0 \tag{14}$$

(13) becomes

$$\text{diag}(\bar{\boldsymbol{v}}^*) \boldsymbol{Y} \boldsymbol{d} = \boldsymbol{s}^*. \tag{15}$$

Let $\bar{\boldsymbol{\rho}} \in \mathbb{R}^N$ be the vector collecting the magnitudes of voltages $\bar{\boldsymbol{v}}$, and define $\bar{\boldsymbol{a}} := \{\cos(\bar{\theta}_n)\}_{n \in \mathcal{N}}$ and $\bar{\boldsymbol{b}} := \{\sin(\bar{\theta}_n)\}_{n \in \mathcal{N}}$ with $\bar{\theta}_i$ being the angle of the nominal voltage $\bar{v}_i$. A solution of (15) can be expressed as $\boldsymbol{d} = \boldsymbol{Y}^{-1} \text{diag}^{-1}(\bar{\boldsymbol{v}}^*) \boldsymbol{s}^*$. Expanding this expression and defining matrices

$$\begin{aligned} \bar{\boldsymbol{R}} &= \boldsymbol{Z}_R \text{diag}(\bar{\boldsymbol{a}})(\text{diag}(\bar{\boldsymbol{\rho}}))^{-1} - \boldsymbol{Z}_I \text{diag}(\bar{\boldsymbol{b}})(\text{diag}(\bar{\boldsymbol{\rho}}))^{-1} \\ \bar{\boldsymbol{B}} &= \boldsymbol{Z}_I \text{diag}(\bar{\boldsymbol{a}})(\text{diag}(\bar{\boldsymbol{\rho}}))^{-1} + \boldsymbol{Z}_R \text{diag}(\bar{\boldsymbol{b}})(\text{diag}(\bar{\boldsymbol{\rho}}))^{-1} \end{aligned} \tag{16}$$

where $\boldsymbol{Z}_R := \Re\{\boldsymbol{Y}^{-1}\}$ and $\boldsymbol{Z}_I := \Im\{\boldsymbol{Y}^{-1}\}$, one can write

$$\boldsymbol{v} \approx \left(\bar{\boldsymbol{R}} + j\bar{\boldsymbol{B}}\right) \boldsymbol{p}_{\text{net}} + \left(\bar{\boldsymbol{B}} - j\bar{\boldsymbol{R}}\right) \boldsymbol{q}_{\text{net}} + \bar{\boldsymbol{v}}. \tag{17}$$

If the entries of $\bar{\boldsymbol{v}}$ dominate those in $\boldsymbol{d}$, then $\boldsymbol{\rho}+\Re\{\boldsymbol{d}\}$ serves as a first-order approximation for the voltage magnitudes. Thus, one can write

$$\hat{H}(\boldsymbol{u};\boldsymbol{p}_l,\boldsymbol{q}_l) := \bar{\boldsymbol{R}}(\boldsymbol{\Gamma}_R\boldsymbol{u}+\boldsymbol{p}_l)+\bar{\boldsymbol{B}}(\boldsymbol{\Gamma}_B\boldsymbol{u}+\boldsymbol{q}_l)+\bar{\boldsymbol{\rho}} \quad (18)$$

with $\boldsymbol{\Gamma}_R \in \mathbb{R}^{N\times 2G}$ and $\boldsymbol{\Gamma}_B \in \mathbb{R}^{N\times 2G}$ matrices filled with 0 and 1 such that $\boldsymbol{\Gamma}_R\boldsymbol{u}+\boldsymbol{p}_l = \boldsymbol{p}_{\text{net}}$ and $\boldsymbol{\Gamma}_B\boldsymbol{u}+\boldsymbol{q}_l = \boldsymbol{q}_{\text{net}}$. Notice that (18) can be written as in (11). Effectively, the approximate Jacobian $J_{\hat{H}} = \bar{\boldsymbol{R}}\boldsymbol{\Gamma}_R + \bar{\boldsymbol{B}}\boldsymbol{\Gamma}_B$ no longer depends on $\boldsymbol{u}$ and the noncontrollable powers $\boldsymbol{p}_l, \boldsymbol{q}_l$; accordingly, it does not need to be recomputed when running (9).

Remark 5 (Validity of the Linear Approximation): The linear model is based on the bus admittance matrix $\boldsymbol{Y}$ and has constant matrices. This approximation is accurate for lightly loaded systems [41]. For heavily loaded systems, [10], [42] showed that feedback-based methods are robust against model mismatch because of the closed-loop implementation; this feature is also pointed out in [34], and our analysis in Section III-C will characterize this robustness. The bus admittance matrix may be hard to obtain because it requires knowledge of the feeder characteristics, i.e., the line impedances, and the network configuration. However, one can assume that the system operator can obtain some estimates. Furthermore, in the case of network reconfiguration, the bus admittance matrix changes, leading to an incorrect linear model. However, this is not a frequent event, and the system operator can update its linear model approximation when such reconfiguration occurs. □

In Section III-C, we analyze the convergence and stability properties of the proposed feedback-based SGF (9).

C. Stability Analysis and Constraint Satisfaction Guarantees

In our technical analysis, we make use of the following assumptions. The assumptions are stated for given values of the noncontrollable powers $\boldsymbol{p}_l, \boldsymbol{q}_l$.

Assumption 3 (Jacobian Errors): $\exists\ E_h < +\infty, E_J < +\infty$ such that $\|\hat{H}(\boldsymbol{u};\boldsymbol{p}_l,\boldsymbol{q}_l) - H(\boldsymbol{u};\boldsymbol{p}_l,\boldsymbol{q}_l)\| \le E_h$ and $\|J_{\hat{H}}(\boldsymbol{u}) - J_H(\boldsymbol{u})\| \le E_J$ for any $\boldsymbol{u} \in \mathcal{B}(\boldsymbol{u}^*, r_1)$. □

Assumption 4 (Measurement Errors): $\exists\ E_M < +\infty$ such that $\|\tilde{\boldsymbol{v}} - \boldsymbol{v}\| \le E_M$. □

Assumptions 3 and 4 are motivated by the following observations: 1) the linear map error $\|\hat{H}(\boldsymbol{u};\boldsymbol{p}_l,\boldsymbol{q}_l) - H(\boldsymbol{u};\boldsymbol{p}_l,\boldsymbol{q}_l)\|$ is bounded and small in a neighborhood of the optimizer (as confirmed in our numerical results and by the analytical findings in [28] and [37]) and 2) in realistic monitoring and SCADA systems, the measurement of the voltage magnitudes are affected by a small (or even negligible) error.

In our analysis, we view (9) as a perturbed version of (7). To begin with, we have the following result.

Lemma 1 (KKT and Equilibrium): Consider the problem (4) satisfying Assumptions 1 and 2. There exists $\boldsymbol{\mu}^*$ such that $(\boldsymbol{u}^*, \boldsymbol{\mu}^*)$ is a KKT point for (4) if and only if $\boldsymbol{u}^*$ is an equilibrium of $\dot{\boldsymbol{u}} = \eta F_\beta(\boldsymbol{u}, H(\boldsymbol{u};\boldsymbol{p}_l,\boldsymbol{q}_l))$. □

Before analyzing the stability of the proposed feedback-based SGF, we provide some notation and intermediate results that will be used in the proof of our main result.

Let $\Omega := J_{\hat{H}}(\boldsymbol{u}) - J_H(\boldsymbol{u})$ and denote by ω_i the ith row of Ω. Moreover, let $\mathbf{e} := \tilde{\boldsymbol{v}} - \boldsymbol{v}$ denote the measurement errors. Then, define $\bar{F}_\beta(\boldsymbol{u}, \Omega, \mathbf{e})$ as

$$\begin{aligned}
&\bar{F}_\beta(\boldsymbol{u}, \Omega, \mathbf{e}) \\
&:= \arg\min_{\boldsymbol{\theta}} \|\boldsymbol{\theta} + \nabla C_p(\boldsymbol{u}) + (J_H(\boldsymbol{u})+\Omega)^\top \nabla C_v(\boldsymbol{v}+\mathbf{e})\|^2 \\
&\quad \text{s.t. } -(\nabla H_i(\boldsymbol{u})+\omega_i)^\top\boldsymbol{\theta} \le -\beta\big(\underline{V} - v_i - e_i\big) \quad \forall i \in \mathcal{M} \\
&\qquad (\nabla H_i(\boldsymbol{u})+\omega_i)^\top\boldsymbol{\theta} \le -\beta\big(v_i + e_i - \bar{V}\big) \quad \forall i \in \mathcal{M} \\
&\qquad J_{\ell_i}(\boldsymbol{u})^\top\theta \le -\beta\ell_i(p_i, q_i) \quad \forall i \in \mathcal{G}
\end{aligned}$$

where $\boldsymbol{v} = H(\boldsymbol{u};\boldsymbol{p}_l,\boldsymbol{q}_l)$. Note that $F_\beta(\boldsymbol{u}, H(\boldsymbol{u};\boldsymbol{p}_l,\boldsymbol{q}_l)) = \bar{F}_\beta(\boldsymbol{u}, \mathbb{0}, \mathbb{0})$ and $\hat{F}_\beta(\boldsymbol{u}, \tilde{\boldsymbol{v}}) = \bar{F}_\beta(\boldsymbol{u}, J_{\hat{H}}(\boldsymbol{u}) - J_H(\boldsymbol{u}), \tilde{\boldsymbol{v}} - \boldsymbol{v})$. Let $\mathcal{E}_J := \{\Omega : \|\Omega\| \le E_J\}$ and $\mathcal{E}_M := \{\mathbf{e} : \|\mathbf{e}\| \le E_M\}$ for brevity. We make the following assumption on $\bar{F}_\beta$.

Assumption 5 (Regularity): For any $\boldsymbol{u} \in \mathcal{B}(\boldsymbol{u}^*, r_1)$, and any Ω and $\mathbf{e}$ satisfying Assumptions 3 and 4, problem (10) is feasible and satisfies the Mangasarian–Fromovitz constraint qualification and the constant-rank condition [43]. □

Since the constraints in the problem defining $\bar{F}_\beta(\boldsymbol{u}, \Omega, \mathbf{e})$ (and, hence, our SGF (9)) are based on techniques from CBFs [24], [25], Assumption 5 guarantees that there always exists a direction for the setpoints to satisfy the constraints of the OPF. Moreover, this assumption allows us to derive the following result.

Lemma 2 (Lipschitz Continuity): Let Assumption 5 hold, and assume that $\boldsymbol{u} \mapsto C_p(\boldsymbol{u})$ and $\boldsymbol{v} \mapsto C_v(\boldsymbol{v})$ are twice continuously differentiable over $\mathcal{B}(\boldsymbol{u}^*, r_1)$ and $\mathcal{V} := \{\boldsymbol{v} \in \mathbb{R}^M : \underline{V} \le v_i + e_i \le \bar{V},\ \forall i \in \mathcal{M}, \boldsymbol{v} = H(\boldsymbol{u};\boldsymbol{p}_l,\boldsymbol{q}_l), \|\mathbf{e}\| \le E_M, \boldsymbol{u} \in \mathcal{B}(\boldsymbol{u}^*, r_1)\}$, respectively. Then, the following holds.

1) For any $\Omega \in \mathcal{E}_J$ and $\mathbf{e} \in \mathcal{E}_M$, $\boldsymbol{u} \mapsto \bar{F}_\beta(\boldsymbol{u}, \Omega, \mathbf{e})$ is locally Lipschitz at $\boldsymbol{u}$, and $\boldsymbol{u} \in \mathcal{B}(\boldsymbol{u}^*, r_1)$.
2) For any $\boldsymbol{u} \in \mathcal{B}(\boldsymbol{u}^*, r_1)$ and $\Omega \in \mathcal{E}_J$, $\mathbf{e} \mapsto \bar{F}_\beta(\boldsymbol{u}, \Omega, \mathbf{e})$ is Lipschitz with constant $\ell_{F_v} \ge 0$ over $\mathcal{E}_M$.
3) For any $\boldsymbol{u} \in \mathcal{B}(\boldsymbol{u}^*, r_1)$ and $\mathbf{e} \in \mathcal{E}_M$, $\Omega \mapsto \bar{F}_\beta(\boldsymbol{u}, \boldsymbol{v}, \Omega, \mathbf{e})$ is Lipschitz with constant $\ell_{F_J} \ge 0$ over $\mathcal{E}_J$. □

Lemma 2 follows from [43, Th. 3.6] and by the compactness of the sets $\mathcal{E}_M$ and $\mathcal{E}_J$. This result ensures the existence and uniqueness of solutions for the proposed feedback-based SGF [44, Ch. 3].

Our main stability result critically relies on these results. Before stating it, we introduce some useful quantities that play a role in the main result; in particular, they are related to local properties of $F_\beta(\boldsymbol{u}, H(\boldsymbol{u};\boldsymbol{p}_l,\boldsymbol{q}_l))$. Recall that $\boldsymbol{u}^*$ is the local optimizer of (4). We define $\boldsymbol{v}^* := H(\boldsymbol{u}^*;\boldsymbol{p}_l,\boldsymbol{q}_l)$, $E := (\partial F_\beta(\boldsymbol{u}, H(\boldsymbol{u};\boldsymbol{p}_l,\boldsymbol{q}_l))/\partial\boldsymbol{u})\ |_{\boldsymbol{u}=\boldsymbol{u}^*}$, $e_1 := -\lambda_{\max}(E)$, and $e_2 := -\lambda_{\min}(E)$. Then, we can write the dynamics as $F_\beta(\boldsymbol{u}, H(\boldsymbol{u};\boldsymbol{p}_l,\boldsymbol{q}_l)) = E(\boldsymbol{u}-\boldsymbol{u}^*) + \hat{g}(\boldsymbol{u})$, where $\hat{g}(u)$ satisfies $\|\hat{g}(\boldsymbol{u})\| \le L\|\boldsymbol{u}-\boldsymbol{u}^*\|^2$, $\forall \boldsymbol{u} \in \mathcal{B}(\boldsymbol{u}^*, r_2)$, for some $L > 0$ and $r_2 > 0$ (see [44]). Define $r := \min\{r_1, r_2\}$ and

$$s_{\min} := \begin{cases} 0, & \text{if } r \ge \dfrac{e_1}{L} \\ 1 - \dfrac{rL}{e_1}, & \text{if } r < \dfrac{e_1}{L}. \end{cases}$$

Since $\mathcal{U}$ is compact, $J_H(\boldsymbol{u})$ is Lipschitz on $\mathcal{U}$ with constant ℓ_H. We are now ready to state the main stability result for (9).

Theorem 1 (Practical Local Exponential Stability): Consider the OPF problem (4) satisfying Assumptions 1 and 2, a linear map $\hat{H}$ satisfying Assumption 3, measurements $\tilde{\boldsymbol{v}}$ satisfying Assumption 4, and the

controller (9) satisfying Assumption 5. Let $\boldsymbol{u}(t)$, $t \geq t_0$, be the unique trajectory of (9). Assume that the set $\mathcal{S} := \{s : s_{\min} < s \leq 1,\ e_1^{-3} e_2 L(\ell_{F_J} E_J + \ell_{F_v} E_M) < s - s^2\}$ is not empty. Then, for any $s \in \mathcal{S}$, it holds that

$$\|\boldsymbol{u}(t) - \boldsymbol{u}^*\| \leq \sqrt{\frac{e_2}{e_1}} e^{-e_1 \eta s (t-t_0)} \|\boldsymbol{u}(t_0) - \boldsymbol{u}^*\| + \frac{e_2(\ell_{F_J} E_J + \ell_{F_v} E_M)}{s e_1^2} \left(1 - e^{-e_1 \eta s (t-t_0)}\right) \tag{19}$$

for any initial condition $\boldsymbol{u}(t_0)$ such that $\|\boldsymbol{u}(t_0) - \boldsymbol{u}^*\| \leq (e_1/e_2)^{1/2}(e_1/L)(1-s)$. △

The proof of the result is provided in Appendix B. The assumption that $\mathcal{S}$ is not empty is necessary to guarantee that the trajectory of $\boldsymbol{u}(t)$ never exits the region of attraction of the optimizer $\boldsymbol{u}^*$. We can notice that the first term on the right-hand side of (19) decays over time; the second term models the effect of the measurement errors and the errors in the computation of the Jacobian. In particular, we can notice that as $t \to +\infty$, the right-hand side of (19) becomes

$$\lim_{t \to +\infty} \|\boldsymbol{u}(t) - \boldsymbol{u}^*\| \leq s^{-1} e_1^{-2} e_2 (\ell_{F_J} E_J + \ell_{F_v} E_M). \tag{20}$$

The asymptotic error can be reduced by increasing the accuracy in the measurement of the voltages (i.e., reducing E_M) or allocating more computational power to compute the Jacobian of the power flow equations (i.e., reducing E_J). The following result characterizes the feasibility of the solution $u(t)$.

Lemma 3 (Practical Forward Invariance): Let the conditions in Theorem 1 be satisfied, and let $\boldsymbol{u}(t)$, $t \geq t_0$, be the unique trajectory of (9) and $\boldsymbol{v}(t)$ be the corresponding voltage magnitudes. Define the set

$$\mathcal{F}_e := \{\boldsymbol{u} : \boldsymbol{u} \in \mathcal{U}, \underline{V}_e \leq H_i(\boldsymbol{u}; \boldsymbol{p}_l, \boldsymbol{q}_l) \leq \bar{V}_e, \forall i \in \mathcal{M}\} \tag{21}$$

with $\underline{V}_e := \underline{V} - E_M - 2E_{\hat{H}}$, $\bar{V}_e := \bar{V} + E_M + 2E_{\hat{H}}$, and $E_{\hat{H}} := \max_{\boldsymbol{u} \in \mathcal{U}} \|\hat{H}(\boldsymbol{u}; \boldsymbol{p}_l, \boldsymbol{q}_l) - H(\boldsymbol{u}; \boldsymbol{p}_l, \boldsymbol{q}_l)\|$. Then, the feedback-based SGF (9) renders a set $\mathcal{F}_s$, with $\mathcal{F} \subseteq \mathcal{F}_s \subseteq \mathcal{F}_e$, forward invariant. □

The proof is provided in Appendix C. Lemma 3 establishes forward invariance of a set $\mathcal{F}_s$, which is a subset of $\mathcal{F}_e$ and inflation of $\mathcal{F}$ (more details about $\mathcal{F}_s$ are provided in the proof); it is clear that $\mathcal{F}_e$ tends to the set $\mathcal{F}$ with the decreasing of the error in the computation of the Jacobian and the measurement errors, which implies that $\mathcal{F}_s$ tends to $\mathcal{F}$ too. If these errors are small, the voltage violation is practically negligible.

In the case of no errors in the measurements and in the computation of the Jacobian, we have the following results.

Corollary 1 (Error-Free Implementation): Let all the conditions in Theorem 1 be satisfied, and assume that there are no measurement errors, i.e., $E_M = 0$, and no errors in the Jacobian, i.e., $E_J = 0$. Let $\boldsymbol{u}(t)$, $t \geq t_0$, be the unique trajectory of (7). Then, it holds that

$$\|\boldsymbol{u}(t) - \boldsymbol{u}^*\| \leq \sqrt{\frac{e_2}{e_1}} \|\boldsymbol{u}(t_0) - \boldsymbol{u}^*\| e^{-e_1 \eta s (t-t_0)}$$

and $\lim_{t \to +\infty} \|\boldsymbol{u}(t) - \boldsymbol{u}^*\| = 0$. △

Lemma 4 (Forward Invariance in Error-Free Implementation): Let the conditions in Theorem 1 be satisfied, and assume that there are no measurement errors (i.e., $E_M = 0$). Let $\boldsymbol{u}(t)$, $t \geq t_0$, be the unique trajectory of (7) and $\boldsymbol{v}(t)$ be the corresponding trajectory of the voltages. Then, (7) renders the set $\mathcal{F}$ forward-invariant. In particular: 1) if $v_i(t_0) \in [\underline{V}, \bar{V}]$, then $v_i(t) \in [\underline{V}, \bar{V}]$ for all $t \geq t_0$ and 2) if $v_i(t_0) \notin [\underline{V}, \bar{V}]$, then there exists $t' \geq t_0$ such that $v_i(t) \in [\underline{V}, \bar{V}]$ for all $t \geq t'$. □

Corollary 1 quantifies the error in the convergence to $\boldsymbol{u}^*$ and certifies local exponential stability properties for the proposed method. Lemma 4 establishes that for the case with no measurement errors and with the exact computation of the Jacobian matrix, the proposed method ensures that voltages are satisfied anytime.

D. Extensions

1) Virtual Power Plants: In this section, we introduce an extension of our formulation for virtual power plants (VPPs). In this case, the goal is to coordinate the operation of the DERs to regulate voltages and provide ancillary services to the bulk power system. In particular, the coordination is to ensure that the active and reactive powers at the substation track a reference $\{P_{0,\text{set}}, Q_{0,\text{set}}\}$. The reference setpoint can be sent by the transmission system operator in order to provide frequency regulation or ancillary services.

Using an expression for the powers at the substation such as $p_0 = G_p(\boldsymbol{u}; \boldsymbol{p}_l, \boldsymbol{q}_l)$ and $q_0 = G_q(\boldsymbol{u}; \boldsymbol{p}_l, \boldsymbol{q}_l)$, the OPF problem in (4) can be extended to include constraints of the form $|(G_p(\boldsymbol{u}; \boldsymbol{p}_l, \boldsymbol{q}_l) - P_{0,\text{set}})| \leq E_p$ and $|(G_q(\boldsymbol{u}; \boldsymbol{p}_l, \boldsymbol{q}_l) - Q_{0,\text{set}})| \leq E_q$, where $E_p > 0$ and $E_q > 0$ are tolerable tracking errors for the setpoints $P_{0,\text{set}}$ and $Q_{0,\text{set}}$, respectively. As an additional example, one can consider the constraint

$$\left\| \begin{bmatrix} G_p(\boldsymbol{u}; \boldsymbol{p}_l, \boldsymbol{q}_l) \\ G_q(\boldsymbol{u}; \boldsymbol{p}_l, \boldsymbol{q}_l) \end{bmatrix} - \begin{bmatrix} P_{0,\text{set}} \\ Q_{0,\text{set}} \end{bmatrix} \right\| \leq E \tag{22}$$

with $E > 0$ again a given tracking error. In the proposed measurement-based SGF, the maps $G_p(\boldsymbol{u}; \boldsymbol{p}_l, \boldsymbol{q}_l)$ and $G_q(\boldsymbol{u}; \boldsymbol{p}_l, \boldsymbol{q}_l)$ would be replaced by measurements of the active and reactive powers at the substation, respectively. Moreover, the Jacobian matrix of $G_p(\boldsymbol{u}; \boldsymbol{p}_l, \boldsymbol{q}_l)$ and $G_q(\boldsymbol{u}; \boldsymbol{p}_l, \boldsymbol{q}_l)$ with respect to $\boldsymbol{u}$ can be approximated by using a linear model [37].

2) Other Constraints: The ac OPF formulation (4) can be extended to include constraints on the power flows or currents. The proposed feedback-based SGF can be naturally modified to enforce constraints on power flows or currents; to this end, one can use a linear model approximating the relationship between power injections at the DERs' nodes and power flows and currents in the controller design [16]. During the operational phase, the controller would rely on measurements of power flows and currents (or measurements) in addition to voltages; see, for example, the discussion in [16].

IV. Numerical Experiments

We consider the medium voltage network (20 kV) shown in Fig. 2(a). We used a modified network from [26], in which PV power plants have been randomly placed, with

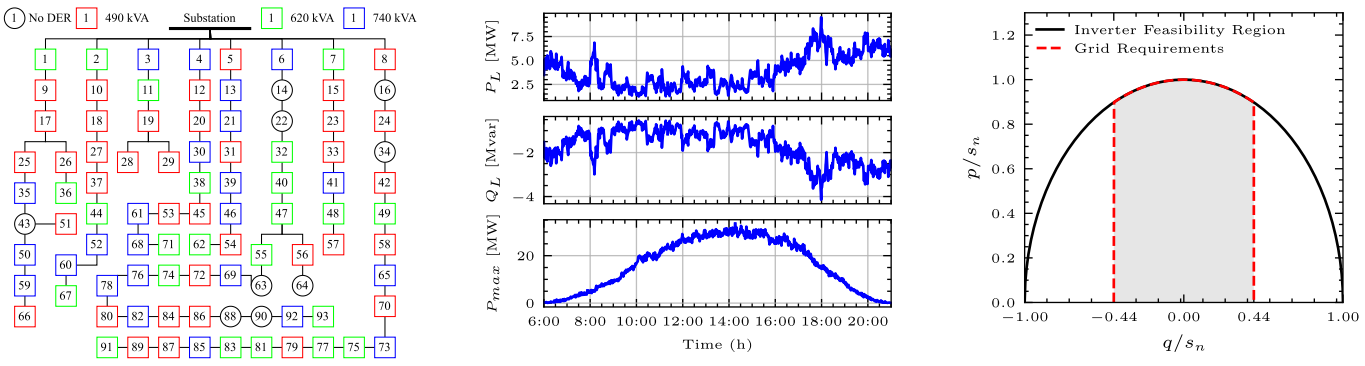

(a) (b) (c)

Fig. 2. (a) Distribution network used in the simulations. (b) Aggregated load consumption (P_L, Q_L) and PV production profiles ($P_{\max}$) used in the simulations. (c) Operational set compared to grid code requirements inspired from the IEEE Std 1547-2018, where s_n is the inverter-rated power.

inverter-rated size picked randomly among $\{490, 620, 740\}$ kVA. The dynamics of the output power for the inverters are not implemented, as they are much faster than the controller dynamics (see, e.g., [45]). Accordingly, when the controller updates the power setpoints, the inverter implements them instantaneously. In the numerical experiments, we consider a system with PV plants; however, we note that any type of inverter-interfaced DERs can be considered. Fig. 2(b) shows the aggregated loads and maximum available active power for PV plants throughout the day. The data are from the Open Power System Data,[1] and have been modified to match the initial loads and PV plants' nominal values present in the network. The reactive power demand is set such that the power factor is 0.9 (lagging). This would represent a typical summer day, with high PV production. We will show that under these conditions, the electrical distribution network would undergo overvoltages.

A. Simulation Setup

We compare the proposed measurement-based SGF with: 1) no control (NC); 2) the online primal-dual method (PDM) proposed in [10]; and 3) a Volt/Var control (VVC). We also compute the solution of a batch optimization (BO) method, where the ac OPF problem, with the power flow equations modeled using the nonlinear branch flow model [46], is solved.

1) Simulation Parameters: The voltage service limits $\bar{V}$ and $\underline{V}$ are set to 1.05 and 0.95 p.u., respectively. The load and PV production profiles have a granularity of 10 s, i.e., active/reactive power consumption and maximum available active power for PV plants change every 10 s. For the SGF, it means that every 10 s, we pursue a new optimal solution. The SGF (using a forward Euler discretization), PDM, and VVC algorithms are run every second.

Based on the IEEE standard *IEEE Std 1547-2018*, we consider the feasible set for the PV plants shown in Fig. 2(c). Although the inverter feasible set consists of a semicircle, there is no interest for PV owners to operate the PV plant at low power factors, i.e., large reactive power absorption/consumption and low active power production. Usually,

[1]Data available at https://data.open-power-system-data.org/household_data/2020-04-15.

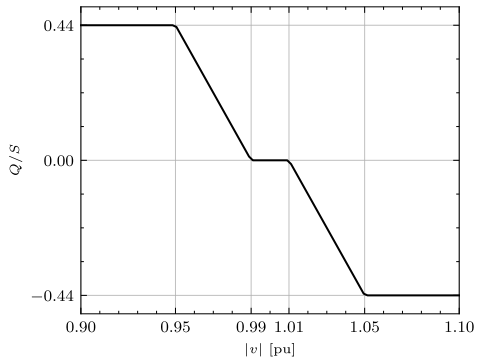

Fig. 3. Implementation of IEEE standard *IEEE Std 1547-2018* with Q being the reactive power injection, S the nominal apparent power of the DER, Q/S the ratio between Q and S, and $|v|$ the voltage magnitude at the node.

PV plants are operated at unity power factor, i.e., on the vertical line passing through 0. The distribution system operator (DSO) often imposes grid requirements when a PV plant is connected to its network in order to provide support if needed. The grid requirements vary from one DSO to another. In this article, we consider that the maximum reactive power that the inverter can produce/consume is set to 44% of its nominal apparent power. The vector-valued function modeling power limits is therefore

$$\ell_i(p_i, q_i) = \begin{bmatrix} p_i^2 + q_i^2 - s_{n,i}^2 \\ p_i - p_{\max,i} \\ -p_i \\ -0.44 s_{n,i} - q_i \\ q_i - 0.44 s_{n,i} \end{bmatrix}. \tag{23}$$

It is assumed that $p_{\max,i}$ is known at the DERs. For example, one can use the method proposed in [47] to estimate the maximum power point of PV arrays and, therefore, the maximum available power $p_{\max,i}$. Finally, we consider the following cost function for the SGF, PDM, and BO:

$$C_P(p_i, q_i) = \sum_{i \in \mathcal{G}} c_p \left(\frac{s_{n,i} - p_i}{s_{n,i}} \right)^2 + c_q \left(\frac{q_i}{s_{n,i}} \right)^2 \tag{24}$$

with $c_p = 3$ and $c_q = 1$. This cost function seeks to minimize active power curtailment and inverter power losses. The first

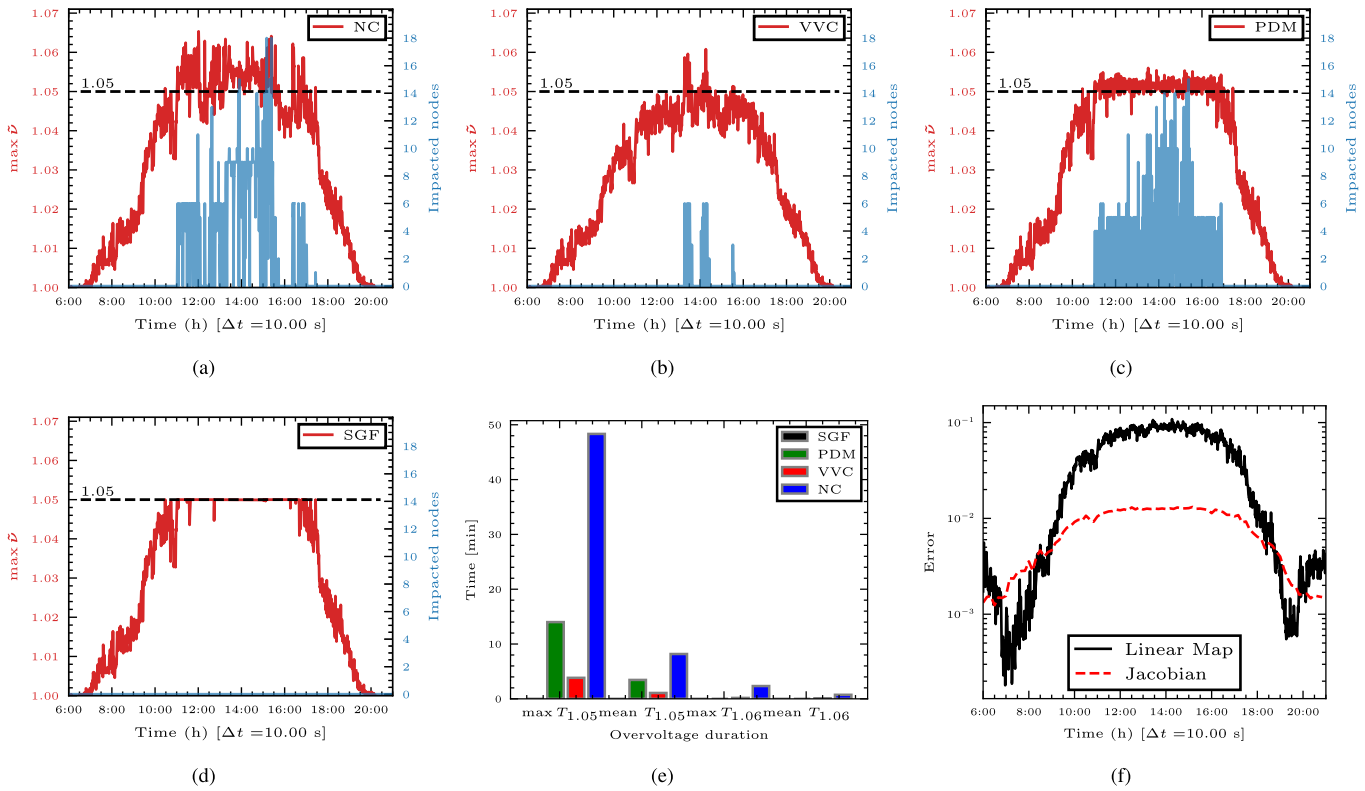

Fig. 4. (a) Overvoltages for NC. (b) Overvoltages for VVC. (c) Overvoltages for PDM. (d) Overvoltages for SGF. (e) Overvoltage duration times. (f) Linear map error: $||\hat{H}(\boldsymbol{u};\boldsymbol{p}_l,\boldsymbol{q}_l) - H(\boldsymbol{u};\boldsymbol{p}_l,\boldsymbol{q}_l)||$ and Jacobian error: $||J_{\hat{H}} - J_H(\boldsymbol{u};\boldsymbol{p}_l,\boldsymbol{q}_l)||$, where $\boldsymbol{u}$ is picked from the SGF algorithm.

part minimizes the active power curtailment, and the second part minimizes the reactive power usage, which is also related to the inverter losses as less reactive power usage means less currents and, thus, less Joules losses.

2) Volt/Var Control: The VVC is inspired by the IEEE standard *IEEE Std 1547-2018*. The parameters of the VVC have been adapted to match the voltage service limits considered in this article. The maximum reactive power consumed/absorbed is set to 44% of the nominal apparent power of the PV plant. The maximum power absorbed/produced is reached for voltages 1.05/0.95 p.u., respectively. Finally, we implemented a deadband for voltages between 0.99 and 1.01 p.u. Our implementation of the IEEE standard *IEEE Std 1547-2018* is shown in Fig. 3.

3) No Control: For the no-control test case, we consider an overvoltage protection of PV plants, i.e., the plant is disconnected if the voltage level is too high. We consider three different statuses for the PV plant: *running*, *idling*, and *disconnected*. When the PV plant is in status *idling* or *disconnected*, it does not inject active power or provide reactive power compensation. The disconnection scheme is inspired by the CENELEC EN50549-2 standard [48] and has been adapted considering the voltage service limits used in this article. The PV plant changes status from *running* to *disconnected* if: 1) the voltage at the point of connection goes above 1.06 p.u. and 2) the root mean square value of the voltages measured at the point of connection for the past 10 min goes above 1.05 p.u. (the voltages are measured every 10 s).

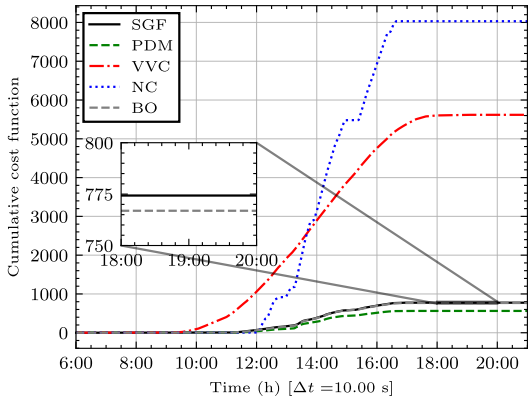

Fig. 5. Achieved values of cumulative cost (24).

The PV plant switches to status *idling* if the voltage at the point of connection stays below 1.05 p.u. for 1 min. To switch back to *running* status, the PV plant has to be in *idling* status. The switching to *running* status occurs randomly in the interval [1, 10 min] (random, uniformly distributed).

B. Results

In the following, we compare the different methods in terms of their cost function values, the system losses, and the voltage levels. Notice that system losses are not integrated into the cost function (24) since they conflict with the term that considers active power curtailment. In this article, we design the cost function to promote renewable energy resources,

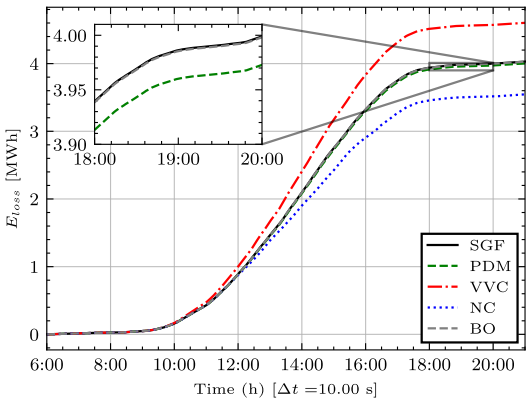

Fig. 6. Sum of energy losses throughout the day.

hence maximizing solar production while keeping voltage levels within predefined bounds. However, the DSO is also concerned by the system losses. Thus, one needs to look at how the different methods perform with respect to them.

1) Voltage Regulation: In Fig. 4, one can see the maximum voltage observed at every time step, as well as the number of impacted nodes where we observed a voltage greater than $\bar{V}$. It can be seen that only the SGF method does not lead to voltage violations. This is precisely because our approach is based on the theory of CBFs. PDM leads to voltage violations not only because of the transient of the dual variables but also because it is designed based on a regularization of the Lagrangian function, as explained in [10]. VVC performs well although, as shown hereafter, it leads to larger system losses and a greater cumulative cost than SGF or PDM. The overall voltage profile is also shifted downward due to its proportional feedback control. One can observe the spikes in the NC method due to multiple disconnections of DERs because of a prolonged overvoltage duration. Finally, one can see that with PDM, the voltages oscillate around the threshold voltage of 1.05 p.u.

2) Overvoltage Duration: In Fig. 4(e), we show the duration of overvoltages. We define $T_{\geq\alpha;i}$ as a vector containing the number of consequent time steps during which node i sees the voltage above the value α. The value max $T_{\geq\alpha}$ corresponds to the maximum value among all $T_{\geq\alpha;i}$ for $i \in \mathcal{N}$ and corresponds to the maximum consequent time duration during which one nodal voltage was above α. The value mean $T_{\geq\alpha}$ is the maximum of the mean absolute values of every vector $T_{\geq\alpha;i}$ for $i \in \mathcal{N}$, representing the average time duration of overvoltage. Since the SGF algorithm does not yield overvoltages, it does not appear on this graph. One can see that the NC method does not perform well, as the active power curtailment is activated only for large overvoltage (above 1.06 p.u.) or for prolonged overvoltage (above 1.05 p.u.).

3) Achieved Cost: We show the cumulative cost function in Fig. 5, i.e., the cumulative sum of the cost function at every time step. It is clear that the NC method leads to the largest cumulative costs, as its implementation leads to full curtailment of solar production and no usage of reactive power. The VVC shows the second highest cost because of its inefficient usage of reactive power reserves. We have to bear in mind that these two solutions cannot practically achieve the optimal solutions of the BO method since they can only play with either the active or reactive power output of solar inverters. Furthermore, they are, by design, decentralized control algorithms and do not have full information on the system state. We observe that PDM has the lowest cumulative cost, which comes at the detriment of voltage violations, as observed in Fig. 4(c). The SGF cumulative cost superposes the BO cost.

4) System Losses: The cumulative system losses for the different methods are shown in Fig. 6. The NC method leads to the lowest system losses as it drastically reduces the amount of active power flows in the network by fully curtailing solar production. The VVC leads to the highest system losses as it overuses reactive power compensation to mitigate voltage issues. This results in larger power flows throughout the network, hence larger power system losses. We can observe that PDM, SGF, and BO have similar system losses.

Finally, Fig. 4(f) shows the error between the linear approximation of the power flow equations and the nonlinear power flow equations, validating our choice for the linear map. It also shows the error between the approximate Jacobian (which is constant) and the true Jacobian computed numerically.

V. Conclusion

This article has addressed the problem of continuously adjusting the power outputs of DERs to pursue feasible solutions of ac OPF problems. We have employed a continuous approximation of projected gradient flows, modified to accommodate voltage measurements from the electrical network, to ensure the satisfaction of voltage constraints at all times. We showed practical exponential stability for scenarios where voltage measurements are subject to errors and where only an approximation of the Jacobian matrix of the power flow equations is available. Our method was experimentally validated on a 93-bus distribution system with realistic load and production profiles. Our approach exhibited a performance significantly superior in terms of voltage regulation to existing online primal-dual methods and Volt/Var strategies. Future research efforts will look at data-driven implementations and event-triggered implementations of the feedback-based SGF.

Appendix

A. CBF-Based Design Principles

In this section, we provide insights into the CBF-based design approach for the proposed measurement-based SGF. Consider rewriting the OPF problem defined in (4) in the following general form:

$$\begin{aligned} &\min_{x\in\mathbb{R}^{2G}} \ f(x) \\ &\text{s.t. } g(x) \leq 0 \end{aligned} \tag{25}$$

with $f : \mathbb{R}^{2G} \to \mathbb{R}$ and $g : \mathbb{R}^{2G} \to \mathbb{R}^P$, where P is the number of voltage and power constraints. Let $\mathcal{F} = \{x \in \mathbb{R}^{2G} \mid g(x) \leq 0\}$ and x^* be a local optimizer of (25). This point, along with

the optimal dual variables $y^* \in \mathbb{R}^P$, satisfies the *Karush–Kuhn–Tucker* conditions

$$\begin{aligned} \nabla f(x^*) + \frac{\partial g(x^*)^\top}{\partial x} y^* &= 0 \\ g(x^*) &\le 0 \\ y^* \ge 0, \quad (y^*)^\top g(x^*) &= 0. \end{aligned} \tag{26}$$

As proposed in [25], the optimization problem (25) can be solved using nonlinear dynamics of the form

$$\dot{x} = -\nabla f(x) - \frac{\partial g(x)^\top}{\partial x} y \tag{27}$$

which can be interpreted as a modification of the gradient flow $-\nabla f(x)$, where the input y can be designed to ensure that the set $\mathcal{F}$ is forward invariant. To this end, define the following admissible set for y:

$$K_\beta(x) := \left\{ y \in \mathbb{R}^P_{\ge 0} \,\middle|\, -\frac{\partial g}{\partial x}\frac{\partial g}{\partial x}^\top y \le \frac{\partial g}{\partial x}\nabla f(x) - \beta g(x) \right\} \tag{28}$$

where $\beta > 0$ is a design parameter, which is inspired by CBF arguments [24] (see [25]). Since we want the drift term $(\partial g(x)^\top/\partial x)y$ as small as possible while ensuring that the set $\mathcal{F}$ is feasible, the input is computed as [25]

$$y(x) = \arg \min_{y \in K_\beta(x)} \left\| \frac{\partial g(x)^\top}{\partial x} y \right\|^2 \tag{29}$$

for each x. The overall modified gradient flow is then given by (27) with the input $y(x)$ in (29).

In [25], it is shown that (27) with the input $y(x)$ in (29) is equivalent to dynamics of the form $\dot{x} = F_\beta(x)$, where the flow $F_\beta(x)$ is defined as

$$\begin{aligned} F_\beta(x) := \arg \min_{\theta \in \mathbb{R}^{2G}} \ & \frac{1}{2}\|\theta + \nabla f(x)\|^2 \\ \text{s.t.} \ & \frac{\partial g(x)}{\partial x}^\top \theta \le -\beta g(x). \end{aligned} \tag{30}$$

In this article, we leverage dynamics of the form (30) to solve our ac OPF problem; however, as explained in Section III, the dynamics are modified to accommodate measurements.

B. Proof of Theorem 1

We recall that $\boldsymbol{v}$ is a short-hand notation for the real voltages, i.e., $\boldsymbol{v} = H(\boldsymbol{u}; \boldsymbol{p}_l, \boldsymbol{q}_l)$, and $\tilde{\boldsymbol{v}}$ is the vector of (pseudo)measurements. Recall also that $F_\beta(\boldsymbol{u}, \boldsymbol{v}) = \bar{F}_\beta(\boldsymbol{u}, \mathbb{0}, \mathbb{0})$ and $\hat{F}_\beta(\boldsymbol{u}, \tilde{\boldsymbol{v}}) = \bar{F}_\beta(\boldsymbol{u}, J_{\hat{H}}(\boldsymbol{u}) - J_H(\boldsymbol{u}), \tilde{\boldsymbol{v}} - \boldsymbol{v})$. First, we express our controller as

$$\begin{aligned} \dot{\boldsymbol{u}} &= \eta \hat{F}_\beta(\boldsymbol{u}, \tilde{\boldsymbol{v}}) \\ &= \eta \bar{F}_\beta(\boldsymbol{u}, \mathbb{0}, \mathbb{0}) \\ &\quad + \eta[\bar{F}_\beta(\boldsymbol{u}, J_{\hat{H}}(\boldsymbol{u}) - J_H(\boldsymbol{u}), \tilde{\boldsymbol{v}} - \boldsymbol{v}) - \bar{F}_\beta(\boldsymbol{u}, \mathbb{0}, \tilde{\boldsymbol{v}} - \boldsymbol{v})] \\ &\quad + \eta[\bar{F}_\beta(\boldsymbol{u}, \mathbb{0}, \tilde{\boldsymbol{v}} - \boldsymbol{v}) - \bar{F}_\beta(\boldsymbol{u}, \mathbb{0}, \mathbb{0})] \end{aligned}$$

where we added and subtracted $\bar{F}_\beta(\boldsymbol{u}, \mathbb{0}, \mathbb{0})$ and $\bar{F}_\beta(\boldsymbol{u}, \mathbb{0}, \tilde{\boldsymbol{v}} - \boldsymbol{v})$, and we reorganized the terms. The feedback-based SGF can then be understood as a perturbation of the nominal gradient flow $\bar{F}_\beta(\boldsymbol{u}, \mathbb{0}, \mathbb{0})$.

By [25, Lemma 5.11 and Th. 5.6(iii)], $\bar{F}_\beta(\boldsymbol{u}, \mathbb{0}, \mathbb{0})$ is differentiable at $\boldsymbol{u}^*$ and its Jacobian $E = (\partial \bar{F}_\beta(\boldsymbol{u}, \mathbb{0}, \mathbb{0})/\partial \boldsymbol{u})\,|_{\boldsymbol{u}=\boldsymbol{u}^*}$ is negative definite. Recall that $e_1 = -\lambda_{\max}(E)$ and $e_2 = -\lambda_{\min}(E)$. Let $P := \int_0^\infty (\exp(E\zeta)^\top \exp(E\zeta) d\zeta$, and then, by [44, Th. 4.12], it holds that $PE + E^\top P = -\mathbf{I}_n$, and $(1/2e_2)\|u - u^*\|_2^2 \le (u - u^*)^\top P(u - u^*) \le (1/2e_1)\|u - u^*\|_2^2$. Let $V_1(\boldsymbol{u}) := (\boldsymbol{u} - \boldsymbol{u}^*)^\top P(\boldsymbol{u} - \boldsymbol{u}^*)$; then, we bound $2(\boldsymbol{u} - \boldsymbol{u}^*)^\top P \bar{F}_\beta(\boldsymbol{u}, \mathbb{0}, \mathbb{0})$ and then leverage this bound to estimate $\dot{V}_1$

$$\begin{aligned} &2(\boldsymbol{u} - \boldsymbol{u}^*)^\top P \bar{F}_\beta(\boldsymbol{u}, \mathbb{0}, \mathbb{0}) \\ &\quad = (\boldsymbol{u} - \boldsymbol{u}^*)^\top \big(PE + E^\top P\big)(\boldsymbol{u} - \boldsymbol{u}^*) \\ &\qquad + 2(\boldsymbol{u} - \boldsymbol{u}^*)^\top P \hat{g}(\boldsymbol{u}) \\ &\quad \le -\|\boldsymbol{u} - \boldsymbol{u}^*\|^2 + \frac{1}{e_1}\|\boldsymbol{u} - \boldsymbol{u}^*\| L \|\boldsymbol{u} - \boldsymbol{u}^*\|^2 \\ &\quad \le \left(-1 + \frac{L}{e_1}\big\|\boldsymbol{u} - \boldsymbol{u}^*\big\|_2\right)\big\|\boldsymbol{u} - \boldsymbol{u}^*\big\|_2^2 \le -s\|\boldsymbol{u} - \boldsymbol{u}^*\|^2 \end{aligned}$$

where the last inequality holds if $\|\boldsymbol{u} - \boldsymbol{u}^*\| \le (e_1/L)(1 - s)$ for any $s \in (s_{\min}, 1]$. Then,

$$\begin{aligned} \dot{V}_1 &= 2(\boldsymbol{u} - \boldsymbol{u}^*)^\top P \dot{\boldsymbol{u}} \\ &= 2\eta(\boldsymbol{u} - \boldsymbol{u}^*)^\top P \bar{F}_\beta(\boldsymbol{u}, \mathbb{0}, \mathbb{0})) + 2\eta(\boldsymbol{u} - \boldsymbol{u}^*)^\top \\ &\quad \times P[\bar{F}_\beta(\boldsymbol{u}, J_{\hat{H}} - J_H, \tilde{\boldsymbol{v}} - \boldsymbol{v}) - \bar{F}_\beta(\boldsymbol{u}, \mathbb{0}, \tilde{\boldsymbol{v}} - \boldsymbol{v})] \\ &\quad + 2\eta(\boldsymbol{u} - \boldsymbol{u}^*)^\top P[\bar{F}_\beta(\boldsymbol{u}, \mathbb{0}, \tilde{\boldsymbol{v}} - \boldsymbol{v}) - \bar{F}_\beta(\boldsymbol{u}, \mathbb{0}, \mathbb{0})] \\ &\le -\eta s\|\boldsymbol{u} - \boldsymbol{u}^*\|^2 + 2\eta\ell_{F_J}\|\boldsymbol{u} - \boldsymbol{u}^*\|\|P\|\|J_H - J_{\hat{H}}\| \\ &\quad + 2\eta\ell_{F_v}\|\boldsymbol{u} - \boldsymbol{u}^*\|\|P\|\|\tilde{\boldsymbol{v}} - \boldsymbol{v}\| \\ &\le -\eta s\|\boldsymbol{u} - \boldsymbol{u}^*\|^2 + \eta\frac{\ell_{F_J}E_J + \ell_{F_v}E_M}{e_1}\|\boldsymbol{u} - \boldsymbol{u}^*\| \\ &\le -2e_1\eta s V_1 + \eta\sqrt{2e_2}\frac{\ell_{F_J}E_J + \ell_{F_v}E_M}{e_1}\sqrt{V_1}. \end{aligned}$$

Define $V_2(\boldsymbol{u}) := \sqrt{V_1(\boldsymbol{u})}$. Then,

$$\begin{aligned} \dot{V}_2 = \frac{\dot{V}_1}{2\sqrt{V_1}} &\le \frac{-2e_1\eta s V_1 + \eta\sqrt{2e_2}\frac{\ell_{F_J}E_J + \ell_{F_v}E_M}{e_1}\sqrt{V_1}}{2\sqrt{V_1}} \\ &= -e_1\eta s V_2 + \eta\sqrt{2e_2}\frac{\ell_{F_J}E_J + \ell_{F_v}E_M}{2e_1}. \end{aligned}$$

In addition, we note that that for any $a \ge 0$, $b > 0$, $y(t) = y(t_0)\exp(-b(t - t_0)) + (a/b)(1 - \exp(-b(t - t_0))$ is the solution of $\dot{y} = -by + a$ and $y(t_0) = y(t_0)$. Hence, by the comparison lemma [44, Lemma 3.4], it follows that

$$\begin{aligned} V_2(t) &\le V_2(t_0)e^{-e_1\eta s(t - t_0)} \\ &\quad + \frac{\sqrt{2e_2}(\ell_{F_J}E_J + \ell_{F_v}E_M)}{2se_1^2}\big(1 - e^{-e_1\eta s(t - t_0)}\big). \end{aligned}$$

Thus, one has that

$$\begin{aligned} \|\boldsymbol{u}(t) - \boldsymbol{u}^*\| &\le \sqrt{2e_2}V_2(t) \\ &\le \sqrt{2e_2}V_2(t_0)e^{-e_1\eta s(t - t_0)} \\ &\quad + \frac{2e_2(\ell_{F_J}E_J + \ell_{F_v}E_M)}{2se_1^2}\big(1 - e^{-e_1\eta s(t - t_0)}\big) \\ &\le \sqrt{\frac{1}{2e_1}}\sqrt{2e_2}e^{-e_1\eta s(t - t_0)}\|\boldsymbol{u}(t_0) - \boldsymbol{u}^*\| \\ &\quad + \frac{e_2(\ell_{F_J}E_J + \ell_{F_v}E_M)}{se_1^2}\big(1 - e^{-e_1\eta s(t - t_0)}\big) \end{aligned}$$

$$= \sqrt{\frac{e_2}{e_1}} e^{-e_1 \eta s (t-t_0)} \|\boldsymbol{u}(t_0) - \boldsymbol{u}^*\| + \frac{e_2(\ell_{F_J} E_J + \ell_{F_v} E_M)}{s e_1^2} \left(1 - e^{-e_1 \eta s (t-t_0)}\right)$$

which proves the result. The limits for $t \to +\infty$ can be computed straightforwardly.

C. Proof of Lemma 3

The proof leverages Nagumo's theorem [49]. For the feedback-based SGF $\hat{F}_\beta(\boldsymbol{u}, \boldsymbol{v})$ in (9), it holds that $-\nabla \hat{H}_i(\boldsymbol{u})^\top \hat{F}_\beta \leq -\beta(\underline{V} - \tilde{v}_i)$. Recall that $\tilde{v}_i = H(\boldsymbol{u}; \boldsymbol{p}_l, \boldsymbol{q}_l) + e_i$ for $i \in \mathcal{M}$. It follows that

$$\begin{aligned}
&-\nabla \hat{H}_i(\boldsymbol{u})^\top \hat{F}_\beta \\
&\leq -\beta\big(\underline{V} - H(\boldsymbol{u}; \boldsymbol{p}_l, \boldsymbol{q}_l) - e_i\big) \\
&= -\beta(\underline{V} - \hat{H}(\boldsymbol{u}; \boldsymbol{p}_l, \boldsymbol{q}_l) - e_i + (H(\boldsymbol{u}; \boldsymbol{p}_l, \boldsymbol{q}_l) - \hat{H}(\boldsymbol{u}; \boldsymbol{p}_l, \boldsymbol{q}_l))) \\
&\leq -\beta((\underline{V} - E_M - E_{\hat{H}}) - \hat{H}(\boldsymbol{u}; \boldsymbol{p}_l, \boldsymbol{q}_l))
\end{aligned}$$

where $E_{\hat{H}} := \max_{\boldsymbol{u} \in \mathcal{U}} \|H(\boldsymbol{u}; \boldsymbol{p}_l, \boldsymbol{q}_l) - \hat{H}(\boldsymbol{u}; \boldsymbol{p}_l, \boldsymbol{q}_l)\|$. Similarly, it also holds that $\nabla \hat{H}_i(\boldsymbol{u})^\top \hat{F}_\beta \leq -\beta(\hat{H}(\boldsymbol{u}; \boldsymbol{p}_l, \boldsymbol{q}_l) - (\bar{V} + E_M + E_{\hat{H}}))$. Thus, the set

$$\mathcal{F}_s := \{\boldsymbol{u} : \underline{V} - E_M - E_{\hat{H}} \leq \hat{H}_i(\boldsymbol{u}; \boldsymbol{p}_l, \boldsymbol{q}_l) \leq \bar{V} + E_M + E_{\hat{H}} \quad \forall i \in \mathcal{M}, \boldsymbol{u} \in \mathcal{U}\}$$

is forward invariant under (9). Note that $\mathcal{F}_s$ is a subset of $\mathcal{F}_e$, and this concludes the proof.

REFERENCES

[1] J. A. Taylor, S. V. Dhople, and D. S. Callaway, "Power systems without fuel," *Renew. Sustain. Energy Rev.*, vol. 57, pp. 1322–1336, May 2016.

[2] B. Kroposki et al., "Autonomous energy grids: Controlling the future grid with large amounts of distributed energy resources," *IEEE Power Energy Mag.*, vol. 18, no. 6, pp. 37–46, Nov. 2020.

[3] Y. Zhu and K. Tomsovic, "Optimal distribution power flow for systems with distributed energy resources," *Int. J. Electr. Power Energy Syst.*, vol. 29, no. 3, pp. 260–267, Mar. 2007.

[4] F. Capitanescu, "Critical review of recent advances and further developments needed in AC optimal power flow," *Electr. Power Syst. Res.*, vol. 136, pp. 57–68, Jul. 2016.

[5] K. Baker, "Emulating AC OPF solvers for obtaining sub-second feasible, near-optimal solutions," 2020, *arXiv:2012.10031*.

[6] R. Nellikkath and S. Chatzivasileiadis, "Physics-informed neural networks for AC optimal power flow," *Electr. Power Syst. Res.*, vol. 212, Nov. 2022, Art. no. 108412.

[7] G. Cheng, Y. Lin, A. Abur, A. Gómez-Expósito, and W. Wu, "A survey of power system state estimation using multiple data sources: PMUs, SCADA, AMI, and beyond," *IEEE Trans. Smart Grid*, vol. 15, no. 1, pp. 1129–1151, Jun. 2023.

[8] C. Muscas, M. Pau, P. A. Pegoraro, and S. Sulis, "Effects of measurements and pseudomeasurements correlation in distribution system state estimation," *IEEE Trans. Instrum. Meas.*, vol. 63, no. 12, pp. 2813–2823, Dec. 2014.

[9] S. Bolognani, R. Carli, G. Cavraro, and S. Zampieri, "Distributed reactive power feedback control for voltage regulation and loss minimization," *IEEE Trans. Autom. Control*, vol. 60, no. 4, pp. 966–981, Apr. 2015.

[10] E. Dall'Anese and A. Simonetto, "Optimal power flow pursuit," *IEEE Trans. Smart Grid*, vol. 9, no. 2, pp. 942–952, Mar. 2018.

[11] A. Hauswirth, S. Bolognani, G. Hug, and F. Dörfler, "Projected gradient descent on Riemannian manifolds with applications to online power system optimization," in *Proc. Annu. Allerton Conf. Commun. Control Comput. (Allerton)*, Sep. 2016, pp. 225–232.

[12] A. Hauswirth, A. Zanardi, S. Bolognani, F. Dörfler, and G. Hug, "Online optimization in closed loop on the power flow manifold," in *Proc. IEEE Manchester PowerTech*, Jun. 2017, pp. 1–6.

[13] S. Nowak, Y. C. Chen, and L. Wang, "A measurement-based gradient-descent method to optimally dispatch DER reactive power," in *Proc. 47th IEEE Photovoltaic Specialists Conf. (PVSC)*, Jun. 2020, pp. 0028–0032.

[14] L. Ortmann, C. Rubin, A. Scozzafava, J. Lehmann, S. Bolognani, and F. Dörfler, "Deployment of an online feedback optimization controller for reactive power flow optimization in a distribution grid," 2023, *arXiv:2305.06702*.

[15] Z. Yuan, G. Cavraro, M. K. Singh, and J. Cortés, "Learning provably stable local Volt/Var controllers for efficient network operation," *IEEE Trans. Power Syst.*, vol. 39, no. 1, pp. 2066–2079, 2024.

[16] A. Bernstein and E. Dall'Anese, "Real-time feedback-based optimization of distribution grids: A unified approach," *IEEE Trans. Control Netw. Syst.*, vol. 6, no. 3, pp. 1197–1209, Sep. 2019.

[17] Y. Chen, A. Bernstein, A. Devraj, and S. Meyn, "Model-free primal-dual methods for network optimization with application to real-time optimal power flow," in *Proc. Amer. Control Conf. (ACC)*, Jul. 2020, pp. 3140–3147.

[18] J. C. Olives-Camps, Á. R. del Nozal, J. M. Mauricio, and J. M. Maza-Ortega, "A model-less control algorithm of DC microgrids based on feedback optimization," *Int. J. Electr. Power Energy Syst.*, vol. 141, Oct. 2022, Art. no. 108087.

[19] L. Gan and S. H. Low, "An Online gradient algorithm for optimal power flow on radial networks," *IEEE J. Sel. Areas Commun.*, vol. 34, no. 3, pp. 625–638, Mar. 2016.

[20] A. Bernstein, L. Reyes-Chamorro, J.-Y. Le Boudec, and M. Paolone, "A composable method for real-time control of active distribution networks with explicit power setpoints. Part I: Framework," *Electr. Power Syst. Res.*, vol. 125, pp. 254–264, Aug. 2015.

[21] Y. Tang, K. Dvijotham, and S. Low, "Real-time optimal power flow," *IEEE Trans. Smart Grid*, vol. 8, no. 6, pp. 2963–2973, Nov. 2017.

[22] J.-L. Lupien, I. Shames, and A. Lesage-Landry, "Online interior-point methods for time-varying equality-constrained optimization," 2023, *arXiv:2307.16128*.

[23] A. Colot, T. Stegen, and B. Cornélusse, "Fully distributed real-time voltage control in active distribution networks with large penetration of solar inverters," in *Proc. IEEE Belgrade PowerTech*, Jun. 2023, pp. 1–6.

[24] A. D. Ames, S. Coogan, M. Egerstedt, G. Notomista, K. Sreenath, and P. Tabuada, "Control barrier functions: Theory and applications," in *Proc. IEEE 18th Eur. Control Conf. (ECC)*, Jun. 2019, pp. 3420–3431.

[25] A. Allibhoy and J. Cortés, "Control-barrier-function-based design of gradient flows for constrained nonlinear programming," *IEEE Trans. Autom. Control*, vol. 69, no. 6, pp. 3499–3514, Jun. 2024.

[26] D. Sarajlic and C. Rehtanz, "Low voltage benchmark distribution network models based on publicly available data," in *Proc. IEEE PES Innov. Smart Grid Technol. Eur. (ISGT-Europe)*, Sep. 2019, pp. 1–5.

[27] W. H. Kersting, *Distribution System Modeling and Analysis*, 2nd ed., Boca Raton, FL, USA: CRC Press, 2007.

[28] S. Bolognani and S. Zampieri, "On the existence and linear approximation of the power flow solution in power distribution networks," *IEEE Trans. Power Syst.*, vol. 31, no. 1, pp. 163–172, Jan. 2016.

[29] A. Bernstein, C. Wang, E. Dall'Anese, J.-Y. L. Boudec, and C. Zhao, "Load flow in multiphase distribution networks: Existence, uniqueness, non-singularity and linear models," *IEEE Trans. Power Syst.*, vol. 33, no. 6, pp. 5832–5843, Nov. 2018.

[30] C. Wang, A. Bernstein, J.-Y. Le Boudec, and M. Paolone, "Existence and uniqueness of load-flow solutions in three-phase distribution networks," *IEEE Trans. Power Syst.*, vol. 32, no. 4, pp. 3319–3320, Jul. 2017.

[31] A. V. Fiacco, "Sensitivity analysis for nonlinear programming using penalty methods," *Math. Program.*, vol. 10, no. 1, pp. 287–311, 1976.

[32] A. Hauswirth, S. Bolognani, G. Hug, and F. Dörfler, "Generic existence of unique Lagrange multipliers in AC optimal power flow," *IEEE Control Syst. Lett.*, vol. 2, no. 4, pp. 791–796, Oct. 2018.

[33] G. Banjac, B. Stellato, N. Moehle, P. Goulart, A. Bemporad, and S. Boyd, "Embedded code generation using the OSQP solver," in *Proc. IEEE 56th Annu. Conf. Decis. Control (CDC)*, Dec. 2017, pp. 1906–1911.

[34] D. K. Molzahn et al., "A survey of distributed optimization and control algorithms for electric power systems," *IEEE Trans. Smart Grid*, vol. 8, no. 6, pp. 2941–2962, Nov. 2017.

[35] M. Picallo, L. Ortmann, S. Bolognani, and F. Dörfler, "Adaptive real-time grid operation via online feedback optimization with sensitivity estimation," *Electr. Power Syst. Res.*, vol. 212, Nov. 2022, Art. no. 108405.

[36] A. M. Ospina and E. Dall'Anese, "Data-driven and online estimation of linear sensitivity distribution factors: A low-rank approach," in *Proc. 62nd IEEE Conf. Decis. Control (CDC)*, Dec. 2023, pp. 7285–7292.
[37] S. V. Dhople, S. S. Guggilam, and Y. C. Chen, "Linear approximations to AC power flow in rectangular coordinates," in *Proc. 53rd Annu. Allerton Conf. Commun., Control, Comput. (Allerton)*, Sep. 2015, pp. 211–217.
[38] V. Kekatos, L. Zhang, G. B. Giannakis, and R. Baldick, "Voltage regulation algorithms for multiphase power distribution grids," *IEEE Trans. Power Syst.*, vol. 31, no. 5, pp. 3913–3923, Sep. 2016.
[39] Y. Sun, X. Chen, S. Yang, K. J. Tseng, and G. Amaratunga, "Micro PMU based monitoring system for active distribution networks," in *Proc. IEEE 12th Int. Conf. Power Electron. Drive Syst. (PEDS)*, Dec. 2017, pp. 518–522.
[40] A. Angioni, T. Schlösser, F. Ponci, and A. Monti, "Impact of pseudo-measurements from new power profiles on state estimation in low-voltage grids," *IEEE Trans. Instrum. Meas.*, vol. 65, no. 1, pp. 70–77, Jan. 2016.
[41] S. Bolognani and F. Dörfler, "Fast power system analysis via implicit linearization of the power flow manifold," in *Proc. Allerton Conf.*, Sep. 2015, pp. 402–409.
[42] L. Ortmann, A. Hauswirth, I. Caduff, F. Dörfler, and S. Bolognani, "Experimental validation of feedback optimization in power distribution grids," *Electr. Power Syst. Res.*, vol. 189, Dec. 2020, Art. no. 106782.
[43] J. Liu, "Sensitivity analysis in nonlinear programs and variational inequalities via continuous selections," *SIAM J. Control Optim.*, vol. 33, no. 4, pp. 1040–1060, 1995.
[44] H. K. Khalil, *Nonlinear Systems*. Upper Saddle River, NJ, USA: Prentice-Hall, 2002.
[45] A. Eggli, S. Karagiannopoulos, S. Bolognani, and G. Hug, "Stability analysis and design of local control schemes in active distribution grids," *IEEE Trans. Power Syst.*, vol. 36, no. 3, pp. 1900–1909, May 2021.
[46] M. E. Baran and F. F. Wu, "Optimal capacitor placement on radial distribution systems," *IEEE Trans. Power Del.*, vol. 4, no. 1, pp. 725–734, Jan. 1989.
[47] A. Hussain, M. M. Garg, M. P. Korukonda, S. Hasan, and L. Behera, "A parameter estimation based MPPT method for a PV system using Lyapunov control scheme," *IEEE Trans. Sustain. Energy*, vol. 10, no. 4, pp. 2123–2132, Oct. 2019.
[48] *Requirements for Generating Plants to be Connected in Parallel With Distribution Networks—Part 2: Connection to a MV Distribution Network—Generating Plants up to and Including Type B*, CENELEC, Brussels, Belgium, 2019, pp. 1–84.
[49] M. Nagumo, "U¨ber die Lage der integralkurven gewöhnlicher differentialgleichungen," *Proc. Physico-Math. Soc. Japan. 3rd Ser.*, vol. 24, pp. 551–559, Jan. 1942.

Antonin Colot (Graduate Student Member, IEEE) received the master's degree in electromechanical engineering from the University of Liège, Liège, Belgium, in 2021, where he is currently pursuing the Ph.D. degree with the Department of Electrical Engineering and Computer Science.

From August 2023 to August 2024, he was a Visiting Student with Prof. Dall'Anese's Group. His research interests span the areas of control of power systems, optimization, and system identification applied to power converters.

Yiting Chen received the master's degree in applied mathematics from The Chinese University of Hong Kong, Hong Kong, in 2022. He is currently pursuing the Ph.D. degree with the Department of Electrical and Computer Engineering, Boston University, Boston, MA, USA.

From 2022 to 2024, he was a Ph.D. Student at the University of Colorado Boulder, Boulder, CO, USA, working with Prof. Dall'Anese's Group. His research interests span the areas of optimization, safe control, and learning.

Bertrand Cornélusse received the M.S. degree in electrical engineering and the Ph.D. degree in engineering sciences from the University of Liège (ULiege), Liège, Belgium, in 2006 and 2010, respectively.

He is an Associate Professor with the Department of Electrical Engineering and Computer Science, ULiège. He specializes in optimizing energy management, including microgrids, distribution systems, and electricity markets.

Jorge Cortés (Fellow, IEEE) received the Licenciatura degree in mathematics from Universidad de Zaragoza, Zaragoza, Spain, in 1997, and the Ph.D. degree in engineering mathematics from the Universidad Carlos III de Madrid, Madrid, Spain, in 2001.

He held postdoctoral positions at the University of Twente, Twente, The Netherlands, and the University of Illinois at Urbana–Champaign, Urbana, IL, USA. He was an Assistant Professor with the Department of Applied Mathematics and Statistics, University of California at Santa Cruz, Santa Cruz, CA, USA, from 2004 to 2007. He is currently a Professor with the Department of Mechanical and Aerospace Engineering, University of California at San Diego, San Diego, CA, USA. His current research interests include distributed control and optimization, network science, resource-aware control, nonsmooth analysis, reasoning and decision-making under uncertainty, network neuroscience, and multiagent coordination in robotic, power, and transportation networks.

Dr. Cortés is a fellow of SIAM and IFAC. At the IEEE Control Systems Society, he was a Distinguished Lecturer from 2010 to 2014, an elected member from 2018 to 2020 of its Board of Governors, and the Director of Operations from 2019 to 2022 of its Executive Committee.

Emiliano Dall'Anese (Senior Member, IEEE) received the Ph.D. degree in information engineering from the Department of Information Engineering, University of Padova, Padua, Italy, in 2011.

He was with the University of Minnesota, Minneapolis, MN, USA, as a Post-Doctoral Researcher, from 2011 to 2014; the National Renewable Energy Laboratory, Golden, CO, USA, as a Senior Researcher, from 2014 to 2018; and the Department of Electrical, Computer, and Energy Engineering, University of Colorado Boulder, Boulder, CO, USA, as a Faculty, from 2018 to 2024. He is an Associate Professor with the Department of Electrical and Computer Engineering, Boston University, Boston, MA, USA, where he is also an Appointed Faculty with the Division of Systems Engineering. He is an Affiliate Faculty with the Center for Information and Systems Engineering and the Institute for Global Sustainability. His research interests span the areas of optimization, control, and learning; current applications include power systems and autonomous systems.

Dr. Dall'Anese received the National Science Foundation CAREER Award in 2020, the IEEE PES Prize Paper Award in 2021, and the IEEE Transactions on Control of Network Systems Best Paper Award in 2023.